

## Article

# Distributed Adaptive NN-Based Attitude Synchronous Tracking Control with Input Saturation

Zhenyu Feng <sup>1</sup> , Jiawei Wang <sup>2,\*</sup>, Neng Wan <sup>3</sup> and Huayi Li <sup>1</sup><sup>1</sup> Research Center of Satellite Technology, Harbin Institute of Technology, Harbin 150001, China<sup>2</sup> Department of Control Science and Engineering, Harbin Institute of Technology, Harbin 150001, China<sup>3</sup> Department of Mechanical Science and Engineering, University of Illinois at Urbana-Champaign, Urbana, IL 61801, USA

\* Correspondence: 11B304008@hit.edu.cn

**Abstract:** The attitude synchronization tracking problem for spacecraft formation flying is investigated in this paper based on sliding-mode control and a Chebyshev neural network (ChNN). A distributed attitude cooperative controller is designed for a group of spacecrafts to guarantee that each individual spacecraft will track the reference attitude of the virtual leader in the presence of external disturbances, system uncertainties and input saturation. An adaptive ChNN is introduced to approximate the system nonlinear uncertainties and bounded external disturbances online, and a switch function, which acts as a switching signal between the adaptive ChNN controller and the robust control law, is applied to limit the output of the ChNN approximator. Then, utilizing Nussbaum-type functions, an auxiliary control system is designed to counteract the nonlinearities caused by input saturation. Finally, a numerical simulation example is provided to illustrate the robustness and effectiveness of the proposed attitude control scheme.

**Keywords:** distributed attitude control; Chebyshev neural network; input saturation; sliding-mode control; Nussbaum-type function



**Citation:** Feng, Z.; Wang, J.; Wan, N.; Li, H. Distributed Adaptive NN-Based Attitude Synchronous Tracking Control with Input Saturation. *Electronics* **2022**, *11*, 4093. <https://doi.org/10.3390/electronics11244093>

Academic Editors: Zhan Li, Zhang Chen and Yiyong Sun

Received: 28 October 2022

Accepted: 5 December 2022

Published: 8 December 2022

**Publisher's Note:** MDPI stays neutral with regard to jurisdictional claims in published maps and institutional affiliations.



**Copyright:** © 2022 by the authors. Licensee MDPI, Basel, Switzerland. This article is an open access article distributed under the terms and conditions of the Creative Commons Attribution (CC BY) license (<https://creativecommons.org/licenses/by/4.0/>).

## 1. Introduction

In the past decade, prompted by the emergence of distributed computation and concepts of cooperation, the technology of spacecraft formation flying (SFF), which coordinates smaller and lower-cost spacecraft to collaboratively accomplish complex and diverse missions, has received sustained attention from many recent researchers. Formation behaviors are abundant in biological systems and artificial machines. Benefiting from advantages such as increased flexibility toward tasks, higher robustness to failures of individual members and better scalability of system deployment [1], SFF has been extensively applied in various space missions, including high resolution imaging, universal exploration, distributed aperture radar, gravitational waves measurement [1–4], etc. Owing to increasingly critical demands on the attitude orientation accuracy in SFF missions, vast research efforts have been dedicated to attitude synchronization and tracking control (ASTC). However, precise attitude control of SFF is still a difficult and open question due to nonlinear characteristics of the attitude dynamics of each spacecraft, limited communication between spacecraft and ineluctable uncertainties such as parametric perturbations, modeling errors and external disturbances. Moreover, considering the physical limitations of actuators, members of a spacecraft formation suffer input saturation in practice, so it is challenging to develop a high-performance attitude synchronization and tracking controller that is robust to the above uncertainties and constraints.

The problem of ASTC is actually a problem of consensus, which aims to synchronize the attitude of spacecraft to a common orientation. Generally, the configuration of the ASTC problem can be classified into one of two strategies: decentralized coordination and distributed coordination. The decentralized coordination strategy, which will not be

discussed in this paper, is based on the premise that the states of the leader or reference desired attitude are accessible to all members in the formation [3,5–7]. On the contrary, the distributed coordination strategy only requires local information from neighbors and the states of the leader are only required by a subset of the followers [4,8–14]. In light of this, the distributed control strategy has stronger robustness, higher efficiency and requires less communication resources [8]. Recently, the graph-theory-based method was used to study the consensus problem by applying local information. In [8], a neural-network-based sliding-mode control (SMC) algorithm was developed for the problem of attitude formation-containment control under directed graph. In the work of Zhu and Guo [9], a distributed adaptive controller was proposed to tackle the ASTC with input saturation. In the work of Zou et al. [11], the problem of velocity-free attitude coordination control under an undirected graph was solved with a finite-time observer and the homogeneous method. To relieve the communication burden, Chen and Shan investigated the attitude regulation of flexible multi-spacecraft under fixed or switching communication graph on SO(3) [12]. Nazari and Butcher [15] studied the consensus control of a rigid-body spacecraft formation with an acyclic directed graph while accounting for a constant communication time delay. In [16], the velocity free leader–follower cooperative attitude tracking problem was investigated under the assumption that the leader–follower graph is a weak tree while the follower graph is undirected.

Disturbance rejection is a commonplace topic in control theory. Due to environmental and structural factors such as solar pressure, aerodynamic drag, gravity gradient torque, sloshing of liquid fuel, vibration of flexible appendages, etc., disturbances are non-ignorable and hard to parameterize [3,9,17]. Moreover, considering the complex communication topology, and the strong coupling and nonlinearity of attitude dynamics, robustness against disturbances and uncertainties is a significant mathematical problem in attitude coordination controller designing [18,19]. Despite the above hardships, numerous control techniques have been studied and are now available in the literature on attitude coordination control, such as adaptive control [3,9,10], observer-based control [11,20], fuzzy control [13,21,22], backstepping control [14,18,23], and event-triggered control [7,24]. Sliding-mode control (SMC), being as one of the variable structure control methods, has attractive features to keep the systems insensitive to matched model uncertainties on the sliding surface, and has been extensively employed in [4,6–8,25–28]. With an increase in research, new SMC-based methods, including terminal SMC [4], integral SMC [25], higher-order SMC [26], fractional-order SMC [27] and optimal SMC [28], are constantly emerging. In recent years, by virtue of its extraordinary capability of universally approximating any smooth function over a compact set [29], the neural network (NN) is increasingly introduced to attitude control in order to counter unknown dynamics [17–19,30–32]. In the work of [18], a radial basis function NN-based optimal adaptive attitude controller was considered to tackle time-varying disturbances. In [19], an actor–critic NN architecture was utilized to compensate system uncertainties online. Zou and Kumar [30] employed the basis functions of the Chebyshev neural network (ChNN) to approximate spacecraft attitude dynamics, and further they extended their work in [31] by proposing a finite-time controller based on a ChNN and terminal SMC. Based on the NN and integral terminal SMC, the problem of angle velocity constrained attitude stabilization is investigated by Yu and Du in [32].

Another crucial issue that deserves attention in control system design is actuator saturation. Limited by space utilization, energy consumption and other realistic factors, an upper magnitude limit on the output of practical actuators always exists. The issue of how to maintain the performance of an attitude control system under actuator saturation is a subject worthy of study. In [4], the controller design procedure was guided by an idea of considering the entire controller as a combination of saturation subsections. The proposed control law was composed of two sub-items, each of whose amplitude range was restrained by a hyperbolic tangent function. A similar thought could be also seen in [2,33,34]. By adopting such techniques, the controller form is simpler by and large, but the actuator's performance is under-utilized [35]. Another prevailing solution is to design

the controller without taking the input saturation into account at first, then take steps to make the obtained controller meet the requirements of saturation [3,9,36,37], but an extra auxiliary control system usually has to be designed to compensate the nonlinearity caused by the saturation constraint, which adds complexity to the controller. Most existing approaches are either conservative or complicated in structure; in consequence, Nussbaum-type functions have attracted increasing attention. The Nussbaum-type function has been broadly employed to deal with systems with unknown control gain [38,39], and it was initially introduced by Wen et al. [40] to compensate the nonlinearity engendered by input saturation, then their works were expended by other researchers [41,42].

Inspired by these works, this paper concentrates on the problem of attitude synchronization and tracking in the presence of external disturbances, inertia uncertainties and input saturation. A novel distributed attitude coordination controller based on the ChNN and Nussbaum gain is proposed and the attitude orientation is described by modified Rodriguez parameters (MRPs). An adaptive ChNN-based approximator, which is a technical extension of the work of Zou et al. [31], is developed to estimate and compensate the uncertainties and unknown nonlinear functions online. Moreover, based on a Nussbaum-type function and a smooth hyperbolic function, an auxiliary virtual control system is devised to handle the nonlinearity arising from input saturation. The main contributions are summarized as follows:

1. The proposed distributed attitude coordination controller for SFF is robust against external disturbances and inertia uncertainties with input saturation. The stability of the controller is verified by Lyapunov's method and the tracking errors are uniformly ultimately bounded (UUB).
2. A ChNN-based approximator, which has the advantages of computational simplicity and easy application [31] is implemented in the proposed controller, and in simulation, it is discovered that chattering caused by the switch function can be avoided by applying a filter.
3. A Nussbaum-type function is introduced to the ASTC to handle the nonlinearity arising from input saturation. This approach can be easily extended to other control problems.

This paper is organized as follows: In Section 2, the problem formula is introduced and the control object is stated. In Section 3, several useful definitions and preliminaries are described. In Section 4, the main results are presented. A distributed adaptive NN-based control law for formation attitude tracking is proposed with a theoretical proof. Simulation results are presented in Section 5 and finally, conclusions are drawn in Section 6.

**Notation:** Throughout the paper, we denote by  $I_n$  the  $n \times n$  identity matrix, and by  $\mathbf{1}_n$  the  $n$ -dimensional column vector with all entries being 1; For any vector  $x \in \mathbb{R}^n$  and matrix  $A \in \mathbb{R}^{n \times n}$ ,  $\|x\|$  and  $\|A\|$  are, respectively, the 2-norm of  $x$  and  $A$ , we define  $\mathcal{F}_D(x) = \text{diag}[\mathcal{F}(x_1), \dots, \mathcal{F}(x_n)] = [\mathcal{F}(x_1), \dots, \mathcal{F}(x_n)]_D$ , where  $\mathcal{F}$  is any given function;  $\otimes$  represents the Kronecker product, and the operator  $(\cdot)^\times \in \mathbb{R}^{3 \times 3}$  denotes the matrix representation of the linear cross-product.

## 2. Problem Statement

### 2.1. Attitude Dynamics of Rigid Spacecraft

For each member of a spacecraft formation system, the attitude kinematics and dynamics described in terms of MRPs can be presented as [8]

$$\dot{\sigma}_i = \mathbf{Z}(\sigma_i)\omega_i \quad (1a)$$

$$\mathbf{J}_i\dot{\omega}_i = -\omega_i^\times \mathbf{J}_i\omega_i + \mathbf{u}_i + \mathbf{d}_i \quad (1b)$$

where  $i = 1, \dots, n$ ;  $\omega_i \in \mathbb{R}^3$  is the angular velocity of the  $i^{\text{th}}$  spacecraft with respect to the inertial frame;  $\mathbf{J}_i \in \mathbb{R}^{3 \times 3}$  denotes the symmetric positive definite inertia tensor;  $\mathbf{u}_i \in \mathbb{R}^3$  is the control torque and  $\mathbf{d}_i \in \mathbb{R}^3$  is the unknown external disturbance torque;  $\sigma_i \in \mathbb{R}^3$  denotes the MRPs representing the attitude orientation of the  $i^{\text{th}}$  spacecraft in the body frame with

respect to the Earth-centered inertial frame, which is a vector defined by  $\sigma_i = \hat{e}_i \tan(\phi_i/4)$ , where  $\hat{e}_i$  and  $\phi_i$  are, respectively, the Euler axis and Euler angle;  $\mathbf{Z}(\sigma)$  is given by [10]

$$\mathbf{Z}(\sigma) = \frac{1}{2} \left( \frac{1 - \sigma^T \sigma}{2} \mathbf{I}_3 + \sigma \sigma^T + \sigma^\times \right)$$

**Remark 1.** In this paper, the MRPs  $\sigma_i$ , rather than the quaternion, are used to describe the attitude kinematics, which is mainly to avoid the undesirable unwinding phenomenon brought by the quaternion. However, it can be seen that MRPs will go singular at  $\phi_i = \pm 360^\circ$ . The singularity problem can be solved by introducing a shadow point of the MRPs vector, which is obtained by  $\sigma_i^s = -(\sigma_i / \sigma_i^T \sigma_i)$ . Readers with an interest in MRPs shadow points can refer to the literature [43,44] and relevant references cited therein.

To investigate the uncertainties of the spacecraft, the following assumptions are made:

**Assumption 1.** The inertia matrix  $\mathbf{J}_i$  is assumed to be in the form of  $\mathbf{J}_i = \mathbf{J}_{0i} + \Delta \mathbf{J}_i$ , where  $\mathbf{J}_{0i}$ , the selected known non-singular symmetric positive definite constant matrix, is the nominal inertia matrix of spacecraft  $i$  and  $\Delta \mathbf{J}_i$  denotes the inertia uncertainty and satisfies  $\|\Delta \mathbf{J}_i\| \leq \lambda_{J_i}$ , where the unknown constant  $\lambda_{J_i} > 0$  is an upper bound on the norm of the inertia uncertainty  $\Delta \mathbf{J}_i$ .

**Assumption 2.** The external disturbance  $\mathbf{d}_i$  in (1b) is assumed to be bounded and satisfies  $\|\Delta \mathbf{d}_i\| \leq \lambda_{d_i}$ , where the unknown constant  $\lambda_{d_i} > 0$  is an upper bound on the norm of the external disturbance  $\mathbf{d}_i$ .

According to Assumption 1 and 2, the dynamic equation set (1) can be rewritten as

$$\dot{\sigma}_i = \mathbf{Z}(\sigma_i) \omega_i \tag{2a}$$

$$\mathbf{J}_{0i} \dot{\omega}_i = -\omega_i^\times \mathbf{J}_{0i} \omega_i + \mathbf{u}_i + \mathbf{d}_i' \tag{2b}$$

where the total uncertainty of the  $i^{th}$  spacecraft  $\mathbf{d}_i' = \mathbf{d}_i - \omega_i^\times \Delta \mathbf{J}_i \omega_i - \Delta \mathbf{J}_i \dot{\omega}_i$  is also bounded.

### 2.2. Actuator with Input Saturation

Taking actuator saturation into consideration,  $\mathbf{u}_i$  can be generally formulated as  $\mathbf{u}_i(\boldsymbol{\tau}_i) = [\text{sat}(\tau_{i,1}), \text{sat}(\tau_{i,2}), \text{sat}(\tau_{i,3})]^T$ , where  $\boldsymbol{\tau}_i$  is the commanded control signal and  $\mathbf{u}_i$  is the actual control torque the constrained system can generate, the function  $\text{sat}(\tau_{i,k})$  is defined as  $\text{sat}(\tau_{i,k}) = \text{sign}(\tau_{i,k}) \cdot \min\{|\tau_{i,k}|, u_{i,k,\max}\}$  ( $k = 1, 2, 3$ ), and  $u_{i,k,\max} > 0$  is the maximum output torque of the corresponding actuator. However, the above saturation function is detrimental to the smoothness of control. To streamline the actuator saturation transition, a hyperbolic tangent function is utilized to design a new commanded control signal [41]

$$\mathbf{u}_i(\boldsymbol{\tau}_i) = \mathbf{g}_i(\boldsymbol{\tau}_i) \tag{3}$$

where  $\mathbf{g}_i(\boldsymbol{\tau}_i) = [g_{i,1}(\tau_{i,1}), g_{i,2}(\tau_{i,2}), g_{i,3}(\tau_{i,3})]^T$ , with  $g_{i,k}(\tau_{i,k}) = u_{i,k,\max} \cdot \tanh(\tau_{i,k}/u_{i,k,\max})$ , owing to the property of the hyperbolic tangent function,  $u_{i,k}(\tau_{i,k})$  tends to  $\pm u_{i,k,\max}$  as  $\tau_{i,k}$  tends to  $\pm\infty$ . More specifically, for any  $\delta > 0$  and  $x \in \mathbb{R}$ , the following formula always holds [45]

$$0 \leq |x| - x \tanh(x/\delta) \leq \kappa \delta, \quad \kappa = 0.2785 \tag{4}$$

On this basis, define the diagonal control matrix  $\mathbf{P}_i = \text{diag}(\rho_{i,1}, \rho_{i,2}, \rho_{i,3})$  with diagonal entries  $\rho_{i,k} = g_{i,k}(\tau_{i,k})/\tau_{i,k}$ . To avoid singularity problems,  $\rho_{i,k} = 1$  when  $\tau_{i,k} = 0$ , and  $\rho_{i,k}$  takes value in the sub-interval of  $[0,1)$ . Thus, considering the actuator saturation, the actual control torque (3) can be rewritten as [36,42]

$$\mathbf{u}_i(\boldsymbol{\tau}_i) = \mathbf{P}_i(\boldsymbol{\tau}_i) \boldsymbol{\tau}_i \tag{5}$$

**Remark 2.** In the light of above definition, the control coefficient matrix  $P_i$  is bounded and time-varying in accordance with  $\tau_i$ . To handle this term, enlightened by article [42], a Nussbaum-type function and related technique is applied. The control error by implementation of (5) can be incorporated into  $d'_i$  and will be handled together in subsequent analysis.

### 2.3. Control Object

Considering the attitude motion function (2), the main control object is to develop an adaptive NN-based control scheme for attitude synchronization and tracking of a spacecraft formation with an undirected communication graph subject to uncertain inertial matrix, external disturbance and input saturation.

## 3. Preliminaries and Lemmas

### 3.1. Graph Theory

In this section, some necessary results from graph theory are introduced to describe the communication topology of a spacecraft formation system [46]. A graph  $\mathcal{G} \triangleq (\mathcal{V}, \mathcal{E}, \mathcal{A})$  is a triple consisting of a vertex set  $\mathcal{V}(\mathcal{G}) = \{v_1, \dots, v_n\}$ , an edge set  $\mathcal{E}(\mathcal{G}) \subset \mathcal{V} \times \mathcal{V}$ , and a relation  $\mathcal{A}$  that associates each edge with an ordered vertex pair  $\langle v_i, v_j \rangle \in \mathcal{E}$ ,  $v_i$  and  $v_j$  are called as the parent vertex and the child vertex, respectively. The neighbor set of  $v_i$  is denoted by  $\mathcal{N}_i = \{v_j : \langle v_i, v_j \rangle \in \mathcal{E}, i \neq j\}$  and  $v_j$  is a neighbor of  $v_i$ . A graph  $\mathcal{G}$  is called undirected if the graph has the property:  $\langle v_i, v_j \rangle \in \mathcal{E} \Leftrightarrow \langle v_j, v_i \rangle \in \mathcal{E}$ , thus an edge in a undirected graph can be denoted by a vertex pair  $(v_i, v_j)$ , which means that the spacecraft  $v_i$  and  $v_j$  can communicate. Similarly, the neighbor set of  $v_i$  in a undirected graph is denoted by  $\mathcal{N}_i = \{v_j : (v_i, v_j) \in \mathcal{E}, i \neq j\}$ .

The adjacency matrix of  $\mathcal{G}$  is the matrix  $A = [a_{ij}] \in \mathbb{R}^{n \times n}$ , where  $a_{ij} > 0$  if  $(v_i, v_j) \in \mathcal{E}$ , while  $a_{ij} = 0$  otherwise. By inspection,  $a_{ij} = a_{ji}$  is valid for an undirected graph. When considering communication, it is realistic to assume there is no loop in the graph, i.e.,  $a_{ii} = 0$ . The in-degree matrix is defined as the diagonal matrix  $\Lambda \in \mathbb{R}^{n \times n}$  with diagonal entries  $d_{ii} = \sum_{j=1}^n a_{ij}$ . The Laplacian matrix  $L \in \mathbb{R}^{n \times n}$  is defined as  $L = \Lambda - A$ . Throughout the paper, the attitude tracking problem of a spacecraft formation with  $n$  members is considered, where the members are in one-to-one correspondence with the vertices of the  $n$ -order graph  $\mathcal{G}$ . If a leader is present in the formation, it is given the index 0; otherwise, we introduce a virtual leader to provide the desired tracking trajectory. The connection matrix  $B \in \mathbb{R}^{n \times n}$ , which is diagonal, indicates the connection between the followers and leader; the diagonal entries  $b_{ii} > 0$  if the  $i^{th}$  spacecraft has access to the leader, otherwise  $b_{ii} = 0$ .

### 3.2. Nussbaum-Type Function

**Definition 1.** [47] Any continuous even function  $N(\chi)$  is called a Nussbaum-type function when it satisfies the following properties

$$\limsup_{r \rightarrow \infty} \frac{1}{r} \int_0^r N(\chi) d\chi = +\infty \tag{6}$$

$$\liminf_{r \rightarrow \infty} \frac{1}{r} \int_0^r N(\chi) d\chi = -\infty \tag{7}$$

Typical choices of Nussbaum-type functions  $N(\chi)$  are  $\chi^2 \cos(\chi)$ ,  $\chi^2 \sin(\chi)$  and  $\exp(\chi^2) \cdot \cos(\frac{d}{w}\chi)$ . However, for a network connected system with multiple subsystems, the traditional Nussbaum-type functions designed for individual systems would not be capable of establishing the boundedness of all the variables in the adaptive consensus control system, it is still not clear how to use traditional Nussbaum-type functions at current stage [38,42,48]. To handle this obstacle, we select the following special Nussbaum-type function [42]

$$N(\chi) = e^{\chi^2/2}(\chi^2 + 2) \sin(\chi) + 1 \tag{8}$$

The Nussbaum function in (8) was originally proposed by Ding [38] and was further modified by Hu in [42].

Together with the Nussbaum-type function (8), some lemmas to be used later are introduced here

**Lemma 1** ([42]). *Let  $V(t)$  and  $\chi_i(t)$  be smooth functions defined on  $[0, t_f)$  with  $V(t) \geq 0$ ,  $\chi_i(0) = 0$  and let  $N(\cdot)$  be a Nussbaum-type function defined by (8). If the following inequality holds*

$$V(t) \leq c_0 + e^{-c_1} \sum_{i=1}^N \int_0^t (-g_i(\tau)N(\chi_i(\tau)) + 1)\dot{\chi}_i(\tau)e^{c_1\tau}d\tau \tag{9}$$

where constant  $c_1 > 0$ , time-varying parameter  $g_i(t)$  takes values in the unknown interval  $I := [g^-, g^+]$  with  $0 \notin I$  and  $c_0$  is a bounded constant, then  $V(t)$ ,  $\chi_i(t)$  and  $\sum_{i=1}^N \int_0^t g_i(\tau)N(\chi_i(\tau)) \cdot \dot{\chi}_i(\tau)d\tau$  are bounded on  $[0, t_f)$ .

**Lemma 2** ([49]). *Let  $f, V : [0, \infty) \mapsto \mathbb{R}$  with  $t_0 \in (0, t)$ , if  $\dot{V} \leq -\alpha V + f$ , constant  $\alpha > 0$ , then*

$$V(t) \leq e^{-\alpha(t-t_0)}V(t_0) + \int_0^t e^{-\alpha(t-\tau)}f(\tau)d\tau \tag{10}$$

**Lemma 3** ([5,50]). *For matrices  $A, B, C$  and  $D$  of appropriate dimensions, the following results hold*

1.  $(\gamma A) \otimes B = A \otimes (\gamma B)$ , where  $\gamma$  is a constant;
2.  $(A + B) \otimes C = A \otimes C + B \otimes C$ ;
3.  $(A \otimes B)(C \otimes D) = (AC) \otimes (BD)$ ;
4. Suppose that  $A$  and  $B$  are invertible, then  $(A \otimes B)^{-1} = (A^{-1}) \otimes (B^{-1})$ ;
5. Let  $\lambda_1, \dots, \lambda_m$  be the eigenvalues of  $A$ , and  $\sigma_1, \dots, \sigma_n$  be those of  $B$ . Then the eigenvalues of  $A \otimes B$  are  $\lambda_i\sigma_j$  ( $i = 1, \dots, m$  and  $j = 1, \dots, n$ ).

**Lemma 4** ([51]). *The Laplace matrix  $L$  in an undirected network  $\mathcal{G}$  has a simple eigenvalue 0 and all the other eigenvalues are positive if and only if the undirected graph is connected.*

**Lemma 5** (Weyl [51]). *Let  $A, B \in \mathbb{R}^{n \times n}$  be Hermitian and let the respective eigenvalues of  $A, B$  and  $A + B$  be  $\{\lambda_i(A)\}_{i=1}^n, \{\lambda_i(B)\}_{i=1}^n$ , and  $\{\lambda_i(A + B)\}_{i=1}^n$ , each algebraically ordered as  $\lambda_{min} = \lambda_1 \leq \lambda_2 \leq \dots \leq \lambda_{n-1} \leq \lambda_n \leq \lambda_{max}$ . Then*

$$\lambda_i(A + B) \leq \lambda_{i+j}(A) + \lambda_{n-j}(B), \quad j = 0, 1, \dots, n - j$$

for each  $i = 1, \dots, n$ , with equality for some pair  $i, j$  if and only if there is a nonzero vector  $x$  such that  $Ax = \lambda_{i+j}(A)x, Bx = \lambda_{n-j}(B)x$  and  $(A + B)x = \lambda_i(A + B)x$ .

Further,

$$\lambda_{i-j+1}(A) + \lambda_j(B) \leq \lambda_i(A + B), \quad j = 1, \dots, i$$

for each  $i = 1, \dots, n$ , with equality for some pair  $i, j$  if and only if there is a nonzero vector  $x$  such that  $Ax = \lambda_{i-j+1}(A)x, Bx = \lambda_j(B)x$  and  $(A + B)x = \lambda_i(A + B)x$ . If  $A$  and  $B$  have no common eigenvector, then every inequality is a strict inequality.

### 3.3. The Chebyshev Neural Network

In this paper, the neural network (NN) structure utilized to approximate the system uncertainties is a single-layer Chebyshev neural network (ChNN). The ChNN is a functional link network based on Chebyshev polynomials [31]. The Chebyshev polynomials have an important application in approximation theory. Chebyshev polynomials of type II  $\mathcal{U}_n(x)$  can be obtained by the two-term recursive formula

$$\begin{cases} \mathcal{U}_0(x) = 1 \\ \mathcal{U}_1(x) = 2x \\ \mathcal{U}_{n+1}(x) = 2x\mathcal{U}_n(x) - \mathcal{U}_{n-1}(x) \end{cases} \quad n \in \mathbb{Z}_+ \quad (11)$$

Based on  $\mathcal{U}_n(x)$ , for a vector  $\mathbf{X} = [x_1, \dots, x_m]^T \in \mathbb{R}^m$  and a continuous nonlinear function  $F(\mathbf{X}) \in \mathbb{R}^n$ ,  $F(\mathbf{X})$  can be approximated by the ChNN as

$$F(\mathbf{X}) = \mathbf{M}^* \Gamma(\mathbf{X}) + \varepsilon \quad (12)$$

where  $\Gamma(\mathbf{X}) = [1, \mathcal{U}_1(x_1), \dots, \mathcal{U}_n(x_1), \dots, \mathcal{U}_1(x_m), \dots, \mathcal{U}_n(x_m)]^T$  is the  $n$ -order Chebyshev polynomial basis function;  $\mathbf{M}^*$  is the unknown optimal weight matrix of appropriate dimension;  $\varepsilon$  denotes the bounded ChNN approximation error.

#### 4. Main Results

In this section, a distributed adaptive NN-based control law is designed for SFF attitude synchronization and tracking under an undirected communication topology in presence of uncertainties and input saturation. A Chebyshev neural network based adaptive controller is implemented to approximate the uncertainties. The input saturation is handled by introducing a Nussbaum function and the Lyapunov method is utilized to analyze the stability of the system.

##### 4.1. Multi-Spacecraft Sliding Manifold Derivation

In this subsection, the multi-spacecraft sliding-mode vector  $\mathbf{S} = [s_1^T, \dots, s_n^T]^T \in \mathbb{R}^{3n}$ ,  $i = 1, \dots, n$  is developed to guarantee the spacecraft formation to achieve attitude synchronous tracking performance, where  $s_i \in \mathbb{R}^3$  is defined as

$$s_i = b_i(\dot{\sigma}_{ei} + k\sigma_{ei}) + \sum_{j=1, j \neq i}^n a_{ij}[(\dot{\sigma}_{ei} + k\sigma_{ei}) - (\dot{\sigma}_{ej} + k\sigma_{ej})] \quad (13)$$

where constant  $k > 0$  and  $a_{ij}, b_i$  are, respectively, elements of the adjacency matrix  $\mathbf{A}$  and the connection matrix  $\mathbf{B}$ , the subscript 0 identifies the desired attitude information, the attitude tracking error of spacecraft  $i$  is defined as  $\sigma_{ei} = \sigma_i - \sigma_0$ , then its derivative  $\dot{\sigma}_{ei} = \dot{\sigma}_i - \dot{\sigma}_0$  obtained. Substituting  $\sigma_{ei}, \dot{\sigma}_{ei}$  into (13) yields

$$\begin{aligned} s_i &= b_i[(\dot{\sigma}_i + k\sigma_i) - (\dot{\sigma}_0 + k\sigma_0)] + \sum_{j=1, j \neq i}^n a_{ij}[(\dot{\sigma}_i + k\sigma_i) - (\dot{\sigma}_j + k\sigma_j)] \\ &= \left( b_i + \sum_{j=1, j \neq i}^n a_{ij} \right) (\dot{\sigma}_i + k\sigma_i) - \sum_{j=1, j \neq i}^n a_{ij} (\dot{\sigma}_j + k\sigma_j) - b_i (\dot{\sigma}_0 + k\sigma_0) \end{aligned} \quad (14)$$

Utilizing the Kronecker product, the sliding-mode vector  $\mathbf{S}$  can be written as

$$\mathbf{S} = [(\mathbf{L} + \mathbf{B}) \otimes \mathbf{I}_3] (\dot{\Sigma}_e + k\Sigma_e) \quad (15)$$

where  $\Sigma_e = [\sigma_1, \dots, \sigma_n]^T$ ,  $\dot{\Sigma}_e = [\dot{\sigma}_1, \dots, \dot{\sigma}_n]^T$ ;  $\mathbf{L}$  and  $\mathbf{B}$  are the Laplacian matrix and the connection matrix that are defined in the previous section. When the sliding-mode vector  $\mathbf{S}$  is zero,  $\dot{\sigma}_{ei} + k\sigma_{ei} = 0$ , thus

$$\lim_{t \rightarrow \infty} \|\sigma_{ei}\| = 0, \quad \lim_{t \rightarrow \infty} \|\dot{\sigma}_{ei}\| = 0, \quad i = 1, \dots, n \quad (16)$$

Therefore, it can be concluded that the attitude tracking errors converge to 0 as  $t \rightarrow \infty$  on the multi-spacecraft sliding-mode manifold  $\mathbf{S} = 0$ . In the final part of this section, the time derivative of  $\mathbf{S}$  is deduced. Taking the time derivative of (13),  $\dot{s}_i$  is given as

$$\dot{s}_i = b_i(\ddot{\sigma}_{ei} + k\dot{\sigma}_{ei}) + \sum_{j=1, j \neq i}^n a_{ij}[(\ddot{\sigma}_{ei} + k\dot{\sigma}_{ei}) - (\ddot{\sigma}_{ej} + k\dot{\sigma}_{ej})] \quad (17)$$

Through the attitude dynamics (2),  $\ddot{\sigma}_{ei} + k\dot{\sigma}_{ei}$  can be obtained

$$\begin{aligned}
 & \ddot{\sigma}_{ei} + k\dot{\sigma}_{ei} \\
 &= \dot{\mathbf{Z}}_i \boldsymbol{\omega}_i + \mathbf{Z}_i \dot{\boldsymbol{\omega}}_i + k\mathbf{Z}_i \boldsymbol{\omega}_i - (\ddot{\sigma}_0 + k\dot{\sigma}_0) \\
 &= \dot{\mathbf{Z}}_i \boldsymbol{\omega}_i + k\mathbf{Z}_i \boldsymbol{\omega}_i - (\ddot{\sigma}_0 + k\dot{\sigma}_0) + \mathbf{Z}_i \mathbf{J}_{0i}^{-1} (-\boldsymbol{\omega}_i^\times \mathbf{J}_{0i} \boldsymbol{\omega}_i + \mathbf{P}_i \boldsymbol{\tau}_i + \mathbf{d}'_i) \\
 &= (\dot{\mathbf{Z}}_i \boldsymbol{\omega}_i + k\mathbf{Z}_i \boldsymbol{\omega}_i - \mathbf{Z}_i \mathbf{J}_{0i}^{-1} \boldsymbol{\omega}_i^\times \mathbf{J}_{0i} \boldsymbol{\omega}_i) - (\ddot{\sigma}_0 + k\dot{\sigma}_0) + \mathbf{Z}_i \mathbf{J}_{0i}^{-1} \mathbf{P}_i \boldsymbol{\tau}_i + \mathbf{Z}_i \mathbf{J}_{0i}^{-1} \mathbf{d}'_i \\
 &= \mathbf{f}_i - \mathbf{f}_0 + \mathbf{q}_i + \mathbf{d}''_i
 \end{aligned} \tag{18}$$

where

$$\begin{cases}
 \mathbf{f}_i = \dot{\mathbf{Z}}_i \boldsymbol{\omega}_i + k\mathbf{Z}_i \boldsymbol{\omega}_i - \mathbf{Z}_i \mathbf{J}_{0i}^{-1} \boldsymbol{\omega}_i^\times \mathbf{J}_{0i} \boldsymbol{\omega}_i \\
 \mathbf{f}_0 = (\ddot{\sigma}_0 + k\dot{\sigma}_0) \\
 \mathbf{q}_i = \mathbf{Z}_i \mathbf{J}_{0i}^{-1} \mathbf{P}_i \boldsymbol{\tau}_i \\
 \mathbf{d}''_i = \mathbf{Z}_i \mathbf{J}_{0i}^{-1} \mathbf{d}'_i \\
 \mathbf{h}_i = \mathbf{f}_i - \mathbf{f}_0
 \end{cases}$$

Substituting (18) into (17), yields

$$\dot{\mathbf{s}}_i = (b_i + \sum_{j=1, j \neq i}^n a_{ij}) (\mathbf{h}_i + \mathbf{q}_i + \mathbf{d}''_i) - \sum_{j=1, j \neq i}^n a_{ij} (\mathbf{h}_j + \mathbf{q}_j + \mathbf{d}''_j) \tag{19}$$

Finally, the time derivative of  $\mathbf{S}$  can be derived from (15) to (19)

$$\dot{\mathbf{S}} = [(\mathbf{L} + \mathbf{B}) \otimes \mathbf{I}_3] (\ddot{\tilde{\mathbf{S}}}_{ei} + k\dot{\tilde{\mathbf{S}}}_{ei}) = [(\mathbf{L} + \mathbf{B}) \otimes \mathbf{I}_3] (\mathbf{H} + \mathbf{Q} + \mathbf{D}) \tag{20}$$

where  $\mathbf{H} = [\mathbf{h}_1^T, \dots, \mathbf{h}_n^T]^T$ ,  $\mathbf{Q} = [\mathbf{q}_1^T, \dots, \mathbf{q}_n^T]^T$ ,  $\mathbf{D} = [\mathbf{d}''_1^T, \dots, \mathbf{d}''_n^T]^T$ .

#### 4.2. Controller Synthesis

For simplification, we start with the hypothesis that the attitude synchronous tracking performance is achievable with a virtual control law  $\mathbf{w}_i$  without considering actuator saturation. Accordingly, by designing the totally same sliding-mode vector as (13) and following the derivation in Section 4.1, the component of corresponding new multi-spacecraft sliding-mode vector  $\tilde{\mathbf{S}}$  with the virtual control law  $\mathbf{w}_i$  is given by

$$\dot{\tilde{\mathbf{s}}}_i = (b_i + \sum_{j=1, j \neq i}^n a_{ij}) (\mathbf{h}_i + \mathbf{w}'_i + \mathbf{d}''_i) - \sum_{j=1, j \neq i}^n a_{ij} (\mathbf{h}_j + \mathbf{w}'_j + \mathbf{d}''_j) \tag{21}$$

where  $\mathbf{w}'_i = \mathbf{Z}_i \mathbf{J}_{0i}^{-1} \mathbf{w}_i$ . Then, following the traditional sliding-mode controller design approach, the control formula can be given conceptually. To organize the derivation process coherently,  $\mathbf{w}'_i$  is divided into two parts

$$\mathbf{w}'_i = \mathbf{w}'_{ia} + \mathbf{w}'_{ib} \tag{22}$$

where  $\mathbf{w}'_{ia} = -\mathbf{h}_i + (b_i + \sum_{j=1, j \neq i}^n a_{ij})^{-1} \sum_{j=1, j \neq i}^n a_{ij} (\mathbf{h}_j + \mathbf{w}'_j)$ , the equivalent control term, is designed to compensate the dynamics of the sliding-mode surface;  $\mathbf{w}'_{ib}$  is the disturbance rejection term to be designed later.

Considering the Lyapunov function candidate  $\tilde{V}_i = \frac{1}{2} \tilde{\mathbf{s}}_i^T \tilde{\mathbf{s}}_i$ , taking the time derivative of  $\tilde{V}_i$  and submitting (21) and (22) yields

$$\begin{aligned}
 \dot{\tilde{V}}_i &= \tilde{\mathbf{s}}_i^T \dot{\tilde{\mathbf{s}}}_i \\
 &= \tilde{\mathbf{s}}_i^T [(b_i + \sum_{j=1, j \neq i}^n a_{ij}) (\mathbf{h}_i + \mathbf{w}'_i + \mathbf{d}''_i) - \sum_{j=1, j \neq i}^n a_{ij} (\mathbf{h}_j + \mathbf{w}'_j + \mathbf{d}''_j)] \\
 &= \tilde{\mathbf{s}}_i^T [(b_i + \sum_{j=1, j \neq i}^n a_{ij}) \mathbf{w}'_{ib} + \boldsymbol{\mu}_i]
 \end{aligned} \tag{23}$$

where

$$\boldsymbol{\mu}_i = (b_i + \sum_{j=1, j \neq i}^n a_{ij}) \mathbf{d}''_i - \sum_{j=1, j \neq i}^n a_{ij} \mathbf{d}''_j \tag{24}$$

**Remark 3.** As  $\mu_i$  is a complex nonlinear state-dependent uncertain term, it is difficult to counteract by direct feedforward compensation. Since the terms constituting  $\mu_i$  are all bounded,  $\mu_i$  is bounded too. Let  $\mu_{i,max}$  denotes the upper bound of  $\|\mu_i\|$ . It follows that  $\mu_i$  can be regarded as a bounded function of  $\lambda_{di}, \lambda_{dj}, \sigma_i, \omega_i, \sigma_j$  and  $\omega_j(j \in \mathcal{N}_i)$  under Assumption 2. To this end, we use a single-layer Chebyshev neural network, which is elaborated in article [31], to approximate  $\mu_i$  and compensate it with a feedback structure.

#### 4.2.1. Control Law Design

In what follows, we present a ChNN scheme based on (12) and (24), which leads to a controller capable of approximating and compensating the uncertain term  $\mu_i$ . Utilizing a ChNN to approximate  $\mu_i$ , taking the following form

$$\mu_i = M_i^* \Gamma_i(X_i) + \varepsilon_i \tag{25}$$

similar to the definitions in Section III,  $X_i = [\sigma_i^T, \omega_i^T, \sigma_j^T, \omega_j^T]^T \in \mathbb{R}^{6 \times (1 + \sum_{j \in \mathcal{N}_i} 1)}$ ,  $\Gamma_i(X_i) = [1, \mathcal{U}_1(X_{i,1}), \dots, \mathcal{U}_n(X_{i,1}), \dots, \mathcal{U}_1(X_{i,end}), \dots, \mathcal{U}_n(X_{i,end})]^T$  is the  $n$ -order Chebyshev polynomial basis function of  $X_i$ ;  $M_i^*$  denotes the unknown optimal weight matrix, using  $\widehat{M}_i$  to represent the estimation of  $M_i^*$ , then the optimal weight estimation error matrix can be denoted  $\widetilde{M}_i = M_i^* - \widehat{M}_i$ ;  $\varepsilon$  denotes the approximation error. Before presenting the designed controller, the following assumptions are required:

**Assumption 3.** The optimal weight matrix  $M_i^*$  is bounded, and there exists a positive constant  $M_{max}$  so that  $\text{Tr}(M_i^{*T} M_i^*) \leq M_{max}$  always holds.

**Assumption 4.** The approximation error  $\varepsilon_i$  is bounded, and there exists a positive constant  $\varepsilon_{i,max}$  so that  $\|\varepsilon_i\| \leq \varepsilon_{max}$  always holds.

Referencing the work in [31], the disturbance compensation term  $w'_{ib}$  of the virtual control law  $w'_i$  is given by

$$w'_{ib} = (b_i + \sum_{j=1, j \neq i}^n a_{ij})^{-1} \varpi_i \tag{26a}$$

$$\varpi_i = -m_i(t)(\widehat{M}_i \Gamma_i + \phi_i) - (1 - m_i(t))\bar{\phi}_i - k_1 s_i - k_2 \text{diag}(|s_i|^{0.5}) \text{sign}(s_i) \tag{26b}$$

$$m_i(t) = \begin{cases} 0, & \|\widehat{M}_i \Gamma_i\| > \mu_{i,max} \\ 1, & \|\widehat{M}_i \Gamma_i\| \leq \mu_{i,max} \end{cases}$$

$$\begin{cases} \phi_i = k_\varepsilon \tanh\left(\frac{3\kappa k_\varepsilon}{\zeta} s_i\right) \\ \bar{\phi}_i = k_\mu \tanh\left(\frac{3\kappa k_\mu}{\zeta} s_i\right) \end{cases}$$

where  $k_1 > 0, k_2 > 0, \zeta > 0, k_\varepsilon > \varepsilon_{max}, k_\mu > \mu_{max}, \kappa = 0.2785$ .  $m_i(t)$  is a switch function, the robust controller  $\phi_i$  and  $\bar{\phi}_i$  are used to compensation the approximation error  $\varepsilon_i$  [21]. The adaptive updating law of  $\widehat{M}_i$  is given as

$$\dot{\widehat{M}}_i = m_i(t) \eta (s_i \Gamma_i^T - \beta \widehat{M}_i) \tag{27}$$

Combining (22) and (26), the virtual control law  $w'_i$  is given by

$$w'_i = -h_i + (b_i + \sum_{j=1, j \neq i}^n a_{ij})^{-1} \left[ \sum_{j=1, j \neq i}^n a_{ij} (h_j + w'_j) + \varpi_i \right] \tag{28}$$

Now the final commanded control signal  $\tau_i$  is synthesized as

$$\tau_i = N_D(\chi_i)w_i \tag{29}$$

$$w_i = J_{0i}Z_i^{-1}\{-f_i + b_i f_0 + (b_i + \sum_{j=1, j \neq i}^n a_{ij})^{-1}[\sum_{j=1, j \neq i}^n a_{ij}(f_j - b_i f_0 + Z_j J_{0j}^{-1}w_j) - m_i(t)(\widehat{M}_i \Gamma_i + \phi_i) - (1 - m_i(t))\bar{\phi}_i - k_1 s_i - k_2 \text{diag}(|s_i|^{0.5})\text{sign}(s_i)]\} \tag{30}$$

$$f_r = \dot{Z}_r \omega_r + k Z_r \omega_r - Z_r J_{0r}^{-1} \omega_r^\times J_{0r} \omega_r \quad (r = i, \text{ or } r \in \mathcal{N}_i) \tag{31}$$

where the feedback gain  $k_1 > 0, k_2 > 0$ , the design parameters  $k_e, k_\mu, \zeta, \eta$  and  $\beta$  have been defined;  $\widehat{M}_i$  is updated by the adaptive updating law (32) with the initial value of 0;  $\chi_i \in \mathbb{R}^3$  obeys the update law (33) and is initialized to 0;  $N_D(\chi_i) = \text{diag}[N(\chi_{i,1}) \ N(\chi_{i,2}) \ N(\chi_{i,3})]$ , of which the elements  $N(\chi_{i,k})$  ( $k = 1, 2, 3$ ) being the Nussbaum-type function are defined by (8), the gain  $\gamma > 0$ .

$$\dot{\widehat{M}}_i = m_i(t)\eta(s_i \Gamma_i^T - \beta \widehat{M}_i) \tag{32}$$

$$\dot{\chi}_i = -\gamma\{[s_i^T(b_i + \sum_{j=1, j \neq i}^n a_{ij}) - \sum_{j=1, j \neq i}^n a_{ij}s_j^T]Z_i J_{0i}^{-1}\}_D w_i \tag{33}$$

To facilitate understanding of the proposed method’s structure, the block diagram of the closed-loop system is illustrated in Figure 1.

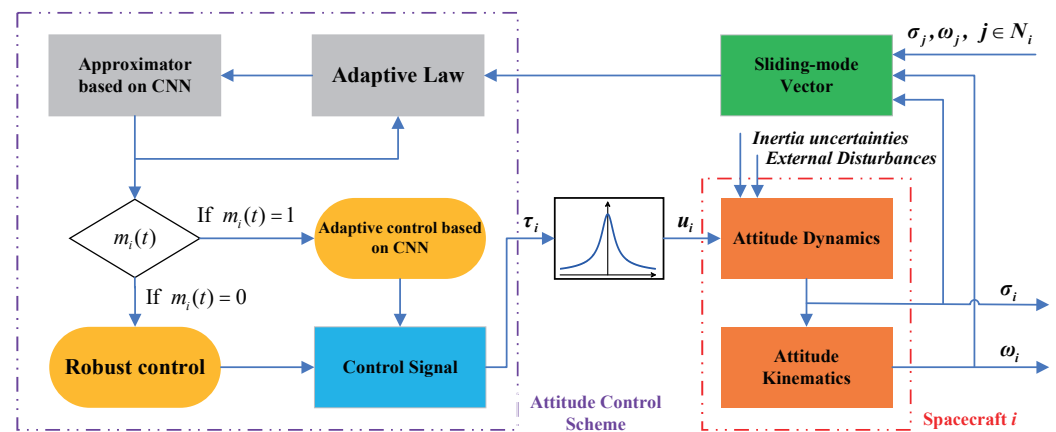


Figure 1. Block diagram of the proposed attitude controller.

**Remark 4.** In the above proposed controller, the Chebyshev neural network is introduced to approximate the uncertainties of the system; however, the estimating ability of the ChNN is generally poor in the learning phase and its output is liable to exceed the bound of the estimated function. To this end, the switch function  $m_i(t)$  is utilized so that the approximator works only when the output of the ChNN is bounded. Moreover, to avoid the chattering phenomenon caused by the utilization of the signum function, the hyperbolic tangent function is applied in the controller [52]. For further understanding, the article [31] elaborates on the functional characteristics of the adaptive ChNN controller.

**Remark 5.** When  $b_i = 0$ , i.e., the  $i^{\text{th}}$  spacecraft does not link to the leader or cannot receive the desired attitude information, according to (14) and (30), it can be obtained that

$$s_i|_{b_i=0} = \sum_{j=1, j \neq i}^n a_{ij}(\dot{\sigma}_i + k\sigma_i) - \sum_{j=1, j \neq i}^n a_{ij}(\dot{\sigma}_j + k\sigma_j)$$

$$w_i|_{b_i=0} = J_{0i}Z_i^{-1}\{-f_i + (\sum_{j=1, j \neq i}^n a_{ij})^{-1}[\sum_{j=1, j \neq i}^n a_{ij}(f_j + Z_j J_{0j}^{-1}w_j) - m_i(t)(\widehat{M}_i \Gamma_i + \phi_i) - (1 - m_i(t))\bar{\phi}_i - k_1 s_i - k_2 \text{diag}(|s_i|^{0.5})\text{sign}(s_i)]\}$$

By adopting the two equations, the desired attitude information can be eliminated from the controller.

### 4.2.2. Stability Analysis

In this part, Lyapunov’s stability method is applied for stability analysis of the closed-loop system.

**Theorem 1.** Consider the spacecraft formation attitude tracking system described by (2) and Assumptions 1–4 are valid, the distributed control law (29) with the adaptive laws (32) and (33) guarantee the  $\sigma_{ei}$  converge to a small region around the equilibrium.

**Proof.** Considering the following Lyapunov function candidate

$$V = \frac{1}{2}S^T S + \frac{1}{2\eta} \sum_{i=1}^n \text{Tr}(\widetilde{M}_i^T \widetilde{M}_i) \tag{34}$$

Let  $W' = [w_1^T, \dots, w_n^T]^T$ , utilizing the Kronecker product and relevant knowledge of graph theory [6,46],  $W'$  can be rewritten as

$$W' = -H + [(\Lambda + B)^{-1} \otimes I_3][(A \otimes I_3)(H + W') + \Pi] \tag{35}$$

where the adjacency matrix  $A$ , the connection matrix  $B$ , the in-degree matrix  $\Lambda$  are defined previously in Section 3,  $H = [h_1^T, \dots, h_n^T]^T$ ,  $\Pi = [\omega_1^T, \dots, \omega_n^T]^T$ . The above equation can be rewritten as

$$W' = -H + \left\{ I_{3n} - [(\Lambda + B)^{-1} \otimes I_3](A \otimes I_3) \right\}^{-1} [(\Lambda + B)^{-1} \otimes I_3] \Pi \tag{36}$$

Since the following equation holds

$$\begin{aligned} & I_{3n} - [(\Lambda + B)^{-1} \otimes I_3](A \otimes I_3) \\ &= [(\Lambda + B)^{-1} \otimes I_3] \{ [(\Lambda + B) \otimes I_3] - (A \otimes I_3) \} \\ &= [(\Lambda + B)^{-1} \otimes I_3] [(L + B) \otimes I_3] \end{aligned}$$

Applying Lemma 3, it can be derived that

$$\begin{aligned} W' &= -H + \{ [(\Lambda + B)^{-1} \otimes I_3] [(L + B) \otimes I_3] \}^{-1} [(\Lambda + B)^{-1} \otimes I_3] \Pi \\ &= -H + [(L + B) \otimes I_3]^{-1} \Pi \end{aligned} \tag{37}$$

Differentiating  $V$  with respect to time and using (20) and (37) yields

$$\begin{aligned} \dot{V} &= S^T \dot{S} - \frac{1}{\eta} \sum_{i=1}^n \text{Tr}(\widetilde{M}_i^T \dot{\widehat{M}}_i) \\ &= S^T [(L + B) \otimes I_3] (H + Q + D) - \frac{1}{\eta} \sum_{i=1}^n \text{Tr}(\widetilde{M}_i^T \dot{\widehat{M}}_i) \\ &= S^T [(L + B) \otimes I_3] (Q - W') + S^T [(L + B) \otimes I_3] (H + W' + D) - \frac{1}{\eta} \sum_{i=1}^n \text{Tr}(\widetilde{M}_i^T \dot{\widehat{M}}_i) \\ &= S^T [(L + B) \otimes I_3] (Q - W') + S^T [(L + B) \otimes I_3] D + S^T \Pi - \frac{1}{\eta} \sum_{i=1}^n \text{Tr}(\widetilde{M}_i^T \dot{\widehat{M}}_i) \end{aligned} \tag{38}$$

here we define that  $\dot{V} = \dot{V}_1 + \dot{V}_2$  with

$$\begin{aligned} \dot{V}_1 &= S^T [(L + B) \otimes I_3] (Q - W') \\ \dot{V}_2 &= S^T [(L + B) \otimes I_3] D + S^T \Pi - \frac{1}{\eta} \sum_{i=1}^n \text{Tr}(\widetilde{M}_i^T \dot{\widehat{M}}_i) \end{aligned}$$

Let us deal with  $\dot{V}_2$  first. Reviewing (24), the expression of  $\mu_i$ , it can be derived that the vector  $N = [\mu_1^T, \dots, \mu_n^T]^T$  is equivalent to  $[(L + B) \otimes I_3] D$ . Submitting  $N$  and the update law (32) of  $\widehat{M}_i$  into  $\dot{V}_2$  yields

$$\begin{aligned}
 \dot{V}_2 &= \mathbf{S}^T \mathbf{N} + \mathbf{S}^T \mathbf{II} - \frac{1}{\eta} \sum_{i=1}^n \text{Tr}(\widehat{\mathbf{M}}_i^T \widehat{\mathbf{M}}_i) \\
 &= \sum_{i=1}^n \mathbf{s}_i^T (\boldsymbol{\mu}_i + \boldsymbol{\omega}_i) - \frac{1}{\eta} \sum_{i=1}^n \text{Tr}(\widehat{\mathbf{M}}_i^T \widehat{\mathbf{M}}_i) \\
 &= \sum_{i=1}^n \mathbf{s}_i^T (\mathbf{M}_i^* \boldsymbol{\Gamma}_i(\mathbf{X}_i) + \boldsymbol{\varepsilon}_i + \boldsymbol{\omega}_i) - \frac{1}{\eta} \sum_{i=1}^n \text{Tr}(\widehat{\mathbf{M}}_i^T \widehat{\mathbf{M}}_i) \\
 &= -k_1 \sum_{i=1}^n \|\mathbf{s}_i\|^2 - k_2 \sum_{i=1}^n \sum_{k=1}^3 |\mathbf{s}_{i,k}|^{\frac{3}{2}} - m_i(t) \sum_{i=1}^n \text{Tr}(\widehat{\mathbf{M}}_i^T \mathbf{s}_i \boldsymbol{\Gamma}_i^T) + m_i(t) \beta \sum_{i=1}^n \text{Tr}(\widehat{\mathbf{M}}_i^T \widehat{\mathbf{M}}_i) \\
 &\quad - m_i(t) \sum_{i=1}^n \mathbf{s}_i^T (\widehat{\mathbf{M}}_i \boldsymbol{\Gamma}_i + \boldsymbol{\phi}_i) - (1 - m_i(t)) \sum_{i=1}^n \mathbf{s}_i^T \bar{\boldsymbol{\phi}}_i + \sum_{i=1}^n \mathbf{s}_i^T (\widehat{\mathbf{M}}_i \boldsymbol{\Gamma}_i + \widehat{\mathbf{M}}_i \boldsymbol{\Gamma}_i + \boldsymbol{\varepsilon}_i) \\
 &\leq -k_1 \|\mathbf{S}\|^2 - k_2 (\|\mathbf{S}\|^2)^{\frac{3}{4}} + \sum_{i=1}^n \mathbf{s}_i^T (\widehat{\mathbf{M}}_i \boldsymbol{\Gamma}_i + \boldsymbol{\varepsilon}_i) + m_i(t) \beta \sum_{i=1}^n \text{Tr}(\widehat{\mathbf{M}}_i^T \widehat{\mathbf{M}}_i) + (1 - m_i(t)) \sum_{i=1}^n \\
 &\quad \cdot \mathbf{s}_i^T \widehat{\mathbf{M}}_i \boldsymbol{\Gamma}_i - m_i(t) \sum_{i=1}^n \mathbf{s}_i^T (\widehat{\mathbf{M}}_i \boldsymbol{\Gamma}_i + \boldsymbol{\phi}_i) - (1 - m_i(t)) \sum_{i=1}^n \mathbf{s}_i^T \bar{\boldsymbol{\phi}}_i
 \end{aligned}$$

where  $\text{Tr}(\widehat{\mathbf{M}}_i^T \mathbf{s}_i \boldsymbol{\Gamma}_i^T) = \text{Tr}(\boldsymbol{\Gamma}_i^T \widehat{\mathbf{M}}_i^T \mathbf{s}_i) = \mathbf{s}_i^T \widehat{\mathbf{M}}_i \boldsymbol{\Gamma}_i$  was used in the above inequality. By applying (4), an algebraic property of the hyperbolic tangent function, it follows that

$$\begin{aligned}
 \dot{V}_2 &\leq -k_1 \|\mathbf{S}\|^2 - k_2 (\|\mathbf{S}\|^2)^{\frac{3}{4}} + m_i(t) \beta \sum_{i=1}^n \text{Tr}(\widehat{\mathbf{M}}_i^T \widehat{\mathbf{M}}_i) + m_i(t) \sum_{i=1}^n \mathbf{s}_i^T (\boldsymbol{\varepsilon}_i - \boldsymbol{\phi}_i) \\
 &\quad - (1 - m_i(t)) \sum_{i=1}^n \mathbf{s}_i^T \bar{\boldsymbol{\phi}}_i + (1 - m_i(t)) \sum_{i=1}^n \mathbf{s}_i^T (\widehat{\mathbf{M}}_i \boldsymbol{\Gamma}_i + \widehat{\mathbf{M}}_i \boldsymbol{\Gamma}_i + \boldsymbol{\varepsilon}_i) \\
 &= -k_1 \|\mathbf{S}\|^2 - k_2 (\|\mathbf{S}\|^2)^{\frac{3}{4}} + m_i(t) \sum_{i=1}^n \mathbf{s}_i^T (\boldsymbol{\varepsilon}_i - \boldsymbol{\phi}_i) + (1 - m_i(t)) \sum_{i=1}^n \mathbf{s}_i^T (\boldsymbol{\mu}_i - \bar{\boldsymbol{\phi}}_i) + \frac{n\beta}{2} M_{\max} \\
 &\leq -k_1 \|\mathbf{S}\|^2 - k_2 (\|\mathbf{S}\|^2)^{\frac{3}{4}} + m_i(t) \sum_{i=1}^n \zeta + (1 - m_i(t)) \sum_{i=1}^n \zeta + \frac{n\beta}{2} M_{\max} \\
 &\leq -k_1 \|\mathbf{S}\|^2 - k_2 (\|\mathbf{S}\|^2)^{\frac{3}{4}} + n\zeta + \frac{n\beta}{2} M_{\max}
 \end{aligned} \tag{39}$$

with the fact that

$$\text{Tr}(\widehat{\mathbf{M}}_i^T \widehat{\mathbf{M}}_i) \leq -\frac{1}{2} \text{Tr}(\widehat{\mathbf{M}}_i^T \widehat{\mathbf{M}}_i) + \frac{1}{2} M_{\max} \leq \frac{1}{2} M_{\max}$$

To facilitate the following working, we define the diagonal matrix  $\mathbf{F} = \text{diag}[J_{01} \mathbf{Z}_1^{-1}, \dots, J_{0n} \mathbf{Z}_n^{-1}]$  and its inverse  $\mathbf{F}^{-1} = \text{diag}[\mathbf{Z}_1 J_{01}^{-1}, \dots, \mathbf{Z}_n J_{0n}^{-1}]$ , then  $\mathbf{W} = [\mathbf{w}_1^T, \dots, \mathbf{w}_n^T]^T$  and  $\mathbf{W}'$  can be linked by  $\mathbf{W}' = \mathbf{F}^{-1} \mathbf{W}$ ; The multi-spacecraft commanded control signal is denoted by  $\mathbf{T} = [\boldsymbol{\tau}_1^T, \dots, \boldsymbol{\tau}_n^T]^T$ , similarly,  $\mathbf{Q} = \mathbf{F}^{-1} \mathbf{P} \mathbf{T}$ , where  $\mathbf{P} = \text{diag}[P_1, \dots, P_n]$ . Since  $\boldsymbol{\tau}_i = N_D(\chi_i) \mathbf{w}_i$ , the equation  $\mathbf{T} = N_D(\boldsymbol{\chi}) \mathbf{W}$  holds, where  $N_D(\boldsymbol{\chi}) = \text{diag}[N_D(\chi_1), \dots, N_D(\chi_n)]$ ,  $\boldsymbol{\chi} = [\chi_1^T, \dots, \chi_n^T]^T$ . Then, looking back to  $\dot{V}_1$ , we obtain

$$\begin{aligned}
 \dot{V}_1 &= \mathbf{S}^T [(\mathbf{L} + \mathbf{B}) \otimes \mathbf{I}_3] (\mathbf{Q} - \mathbf{W}') \\
 &= \mathbf{S}^T [(\mathbf{L} + \mathbf{B}) \otimes \mathbf{I}_3] \mathbf{F}^{-1} (\mathbf{P} N_D(\boldsymbol{\chi}) - \mathbf{I}_{3n}) \mathbf{W} \\
 &= -\frac{1}{\gamma} \mathbf{S}^T [(\mathbf{L} + \mathbf{B}) \otimes \mathbf{I}_3] \mathbf{F}^{-1} \{ \mathbf{S}^T [(\mathbf{L} + \mathbf{B}) \otimes \mathbf{I}_3] \mathbf{F}^{-1} \}_D^{-1} (\mathbf{P} N_D(\boldsymbol{\chi}) - \mathbf{I}_{3n}) \boldsymbol{\chi} \\
 &= -\frac{1}{\gamma} \mathbf{1}_{3n}^T ((\mathbf{P} N_D(\boldsymbol{\chi}) - \mathbf{I}_{3n}) \boldsymbol{\chi}) \\
 &= -\frac{1}{\gamma} \sum_{i=1}^n \sum_{k=1}^3 (\rho_{i,k} N(\chi_{i,k}) - 1) \dot{\chi}_{i,k}
 \end{aligned} \tag{40}$$

Combining (39) and (40), it can be obtained that

$$\begin{aligned}
 \dot{V} &\leq -\frac{1}{\gamma} \sum_{i=1}^n \sum_{k=1}^3 (\rho_{i,k} N(\chi_{i,k}) - 1) \dot{\chi}_{i,k} - k_1 \|\mathbf{S}\|^2 - k_2 (\|\mathbf{S}\|^2)^{\frac{3}{4}} + n\zeta + \frac{n\beta}{2} M_{\max} \\
 &= \alpha V - \frac{1}{\gamma} \sum_{i=1}^n \sum_{k=1}^3 (\rho_{i,k} N(\chi_{i,k}) - 1) \dot{\chi}_{i,k} + \Delta
 \end{aligned} \tag{41}$$

where  $\alpha = 2k_1$ ,  $\Delta = n\zeta + \frac{n}{2} \left( \beta + \frac{2k_1}{\eta} \right) M_{\max}$ . According to Lemma 3, the above differential inequality can be solved as

$$V(t) \leq e^{-\alpha t} \int_0^t \frac{1}{\gamma} \sum_{i=1}^n \sum_{k=1}^3 (-\rho_{i,k} N(\chi_{i,k}) + 1) \dot{\chi}_{i,k} e^{-\alpha \tau} d\tau + e^{-\alpha t} \left( V(0) - \frac{\Delta}{\alpha} \right) + \frac{\Delta}{\alpha} \tag{42}$$

It is not difficult to verify that the function  $e^{-\alpha t} \left( V(0) - \frac{\Delta}{\alpha} \right) + \frac{\Delta}{\alpha}$  is bounded and tends to  $\frac{\Delta}{\alpha}$  on  $[0, t_f]$  and  $\alpha = 2k_1 > 0$ . Based on Lemma 1, we can draw the conclusion that  $V(t)$ ,

$\chi_{i,k}$  and  $\int_0^t \frac{1}{\gamma} \sum_{i=1}^n \sum_{k=1}^3 (-\rho_{i,k} N(\chi_{i,k}) + 1) \dot{\chi}_{i,k} e^{-\alpha\tau} d\tau$  are bounded. The fractional-order sliding-mode term is applied to accelerate the convergence of  $s_i$ . We can further obtain that  $s_i, \sigma_{ei}, \dot{\sigma}_{ei}$  are all bounded.

For convenience of analysis, the upper bound of  $V(t)$  and  $\int_0^t \frac{1}{\gamma} \sum_{i=1}^n \sum_{k=1}^3 (-\rho_{i,k} N(\chi_{i,k}) + 1) \dot{\chi}_{i,k} e^{-\alpha\tau} d\tau$  are, respectively, denoted as  $V_{\max}$  and  $c_{\max}$ , Equation (42) reduces to

$$V(t) \leq \lambda_1 + e^{-\alpha t}(V(0) - \lambda_2) = V_{\max}$$

where  $\lambda_1 = \lambda_2 + c_{\max} e^{-\alpha t}$ ,  $\lambda_2 = \frac{\Delta}{\alpha}$ , so the multi-spacecraft sliding manifold will converge to  $\|S\| \leq \sqrt{2(\lambda_1 + e^{-\alpha t}(V(0) - \lambda_2))}$ , it is noticed that  $e^{-\alpha t}(V(0) - \lambda_2)$  is monotonically decreasing on  $[0, t_f)$ , thus the convergence region tends to  $\Omega_s = \{S \mid \|S\| \leq \sqrt{2\lambda_1}\}$  over time, thus it is proven the sliding mode vector  $S$  is uniformly ultimately bounded. As stated in the definition of  $S$  in (15), we can obtain that  $\|\dot{\sigma}_{ei} + k\sigma_{ei}\| < c_{\mathcal{G}}\Delta_s$ , where  $\Delta_s$  denotes the convergence region radius of  $S$  and the constant  $c_{\mathcal{G}} > 0$ , it can be derived that the attitude error  $\sigma_{ei}$  will converge to  $\|\sigma_{ei}\| \leq c_{\mathcal{G}}\Delta_s/k$ .  $\square$

**Remark 6.** It should be noticed that the structure of the formation communication topology has a bearing on the convergence region size of  $\sigma_{ei}$ . According to Equation (15), the definition of sliding-mode vector  $S$ , we have  $\|\dot{\Sigma}_e + k\Sigma_e\| \leq \|[(L + B) \otimes I_3]^{-1}\| \times \|S\|$ , in view that  $(L + B)$  is Hermitian under an undirected connected graph,  $\|\dot{\Sigma}_e + k\Sigma_e\| \leq \Delta_s/\rho(L + B) = \Delta_s/\lambda_{\min}(L + B)$ , i.e.,  $c_{\mathcal{G}} = 1/\lambda_{\min}(L + B)$  and  $\rho(L + B)$  denote the spectral radius of the matrix  $(L + B)$ , where Lemmas 4 and 5 and the property 5) of Lemma 3 are applied. The positivity of  $\lambda_{\min}(L + B)$  can be guaranteed by the Weyl theorem. We can first obtain that  $\lambda_{\min}(L + B) = \lambda_1(L + B) \leq \lambda_1(L) + \lambda_1(B) = 0$ . Since  $L$  has the property that  $\sum_{j=1}^n L_{ij} = 0$ , it is obvious that  $\mathbf{1}_n$  is the eigenvector of  $L$  associated with the simple eigenvalue 0, the equality holds if and only if the connection matrix  $B$  is the zero matrix, which implies that there is no desired attitude to be tracking. The minimum eigenvalue of  $(L + B)$  has an important influence on the convergence accuracy of  $\sigma_{ei}$ —a reasonable designed communication topology is conducive to improving control accuracy.

### 5. Simulation Results

In this section, the effectiveness and performance of the proposed distributed control law on spacecraft formation attitude tracking is verified through numerical simulations, where a scenario of a micro-spacecraft formation consists of four follower spacecraft and one virtual leader under the interaction topology shown in Figure 2, which is undirected. The reference attitude trajectory is given by the initial attitude  $\sigma_0 = [0, 0, 0]^T$  and the desired angular velocity  $\omega_0(t) = [0.08 \sin(\pi t/60), 0.1 \cos(\pi t/60 + \pi/6), 0.06 \sin(\pi t/60 - \pi/4)]^T$ . The inertia matrices of the spacecraft are chosen differently and listed in Table 1, the initial attitudes are  $[0.0655, 0, 0]^T$ ,  $[0.0758, -0.0506, 0.0607]^T$ ,  $[0.0556, -0.0404, -0.0758]^T$ ,  $[0.2764, -0.5528, 0]^T$ , their initial angular velocities are supposed to be zero, i.e.,  $\omega_0 = 0$ ,  $i = 1, 2, 3, 4$ .

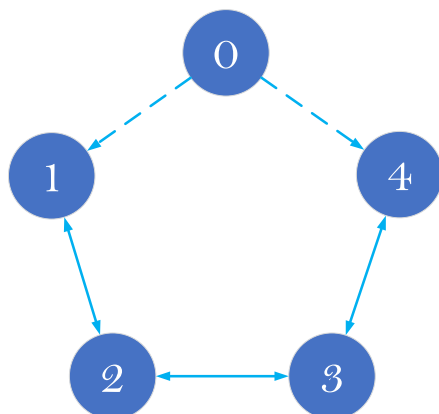


Figure 2. Communication topology.

**Table 1.** Simulation settings.

| $n$ | Inertia Matrix   | Inertia Uncertainty  | External Disturbance  |
|-----|--|--|---|
|     | ( $\text{kg} \cdot \text{m}^2$ )                                       | ( $\text{kg} \cdot \text{m}^2$ )   | (Nm)  |
| 1   | $\begin{bmatrix} 22 & 0 & 0 \\ 0 & 19 & 0 \\ 0 & 0 & 18 \end{bmatrix}$ | $\sin(0.04t) \begin{bmatrix} 1.1 & 0.8 & 0.9 \\ 0.8 & 0.95 & 0.7 \\ 0.9 & 0.7 & 0.9 \end{bmatrix}$   | $0.005 \begin{bmatrix} 0.3 \cos(0.04t) + 0.6 \\ 0.7 \sin(0.04t) - 0.5 \\ 0.7 \sin(0.04t) - 0.2 \end{bmatrix}$ |
| 2   | $\begin{bmatrix} 21 & 0 & 0 \\ 0 & 19 & 0 \\ 0 & 0 & 17 \end{bmatrix}$ | $\sin(0.04t) \begin{bmatrix} 1.05 & 1.2 & 0.6 \\ 1.2 & 0.95 & 0.3 \\ 0.6 & 0.3 & 0.85 \end{bmatrix}$ | $0.005 \begin{bmatrix} 0.7 \sin(0.05t) + 0.2 \\ 0.3 \cos(0.05t) - 0.2 \\ 0.7 \sin(0.05t) + 0.6 \end{bmatrix}$ |
| 3   | $\begin{bmatrix} 20 & 0 & 0 \\ 0 & 18 & 0 \\ 0 & 0 & 19 \end{bmatrix}$ | $\sin(0.04t) \begin{bmatrix} 1 & 0.9 & 0.6 \\ 0.9 & 0.9 & 0.5 \\ 0.6 & 0.5 & 0.95 \end{bmatrix}$     | $0.005 \begin{bmatrix} 0.3 \sin(0.06t) + 0.4 \\ 0.7 \sin(0.06t) - 0.5 \\ 0.3 \cos(0.06t) - 0.6 \end{bmatrix}$ |
| 4   | $\begin{bmatrix} 20 & 0 & 0 \\ 0 & 18 & 0 \\ 0 & 0 & 18 \end{bmatrix}$ | $\sin(0.04t) \begin{bmatrix} 1 & 1 & 0.8 \\ 1 & 0.9 & 0.4 \\ 0.8 & 0.4 & 0.9 \end{bmatrix}$          | $0.005 \begin{bmatrix} 0.6 \cos(0.07t) - 0.3 \\ 0.2 \sin(0.07t) - 0.4 \\ 0.7 \cos(0.07t) + 0.2 \end{bmatrix}$ |

In order to verify the robustness of the proposed controller against the inertia uncertainty and external disturbance, a margin of error of about 5 percent is added to the inertia matrix such as what article [3] achieved. The inertia uncertainties and external disturbances are listed in Table 1. In addition, considering the constraint of input saturation, the actual control torque is bound by  $u_{i,k,\max} = 0.3 \text{ Nm}$  for simulation purposes.

For the purpose of investigating the control performance of the proposed controller, two indexes including the mean square of the tracking error (MSTE) and the mean square of the control torque (MSCT) are introduced from Ref. [31] as follows

$$\text{MSTE} = \frac{\sum_{i=1}^N \int_0^T \|\sigma_{ei}\|^2 dt}{N \cdot T}$$

$$\text{MSCT} = \frac{\sum_{i=1}^N \int_0^T \|\mathbf{u}_i\|^2 dt}{N \cdot T}$$

These indexes can estimate the efficiency of controllers to a certain extent. The values of these two indexes are summarized in Table 2 and  $T = 200 \text{ s}$  is selected for all cases in the simulation.

The attitude MRPs tracking errors, angle velocity tracking errors and attitude synchronization performance are depicted, respectively, in Figures 3–5, which show that the proposed adaptive NN-based attitude controller can guarantee system stabilization and realize the formation attitude synchronization and tracking performance in spite of inertia uncertainty, external disturbance and input saturation. As it happened, the simulation did not suffer from the attitude MRPs singularity problem; thus, the switch between MRPs and their shadow set was not taken into consideration when drawing Figure 5 for convenience.

**Table 2.** Performance indexes for the controllers.

| Controller                | MSTE   | MSCT ( $\text{N}^2 \cdot \text{m}^2$ ) |
|---------------------------|--------|--|
| The proposed controller   | 0.0061 | 0.0254                                 |
| The comparison controller | 0.1405 | 0.0427                                 |

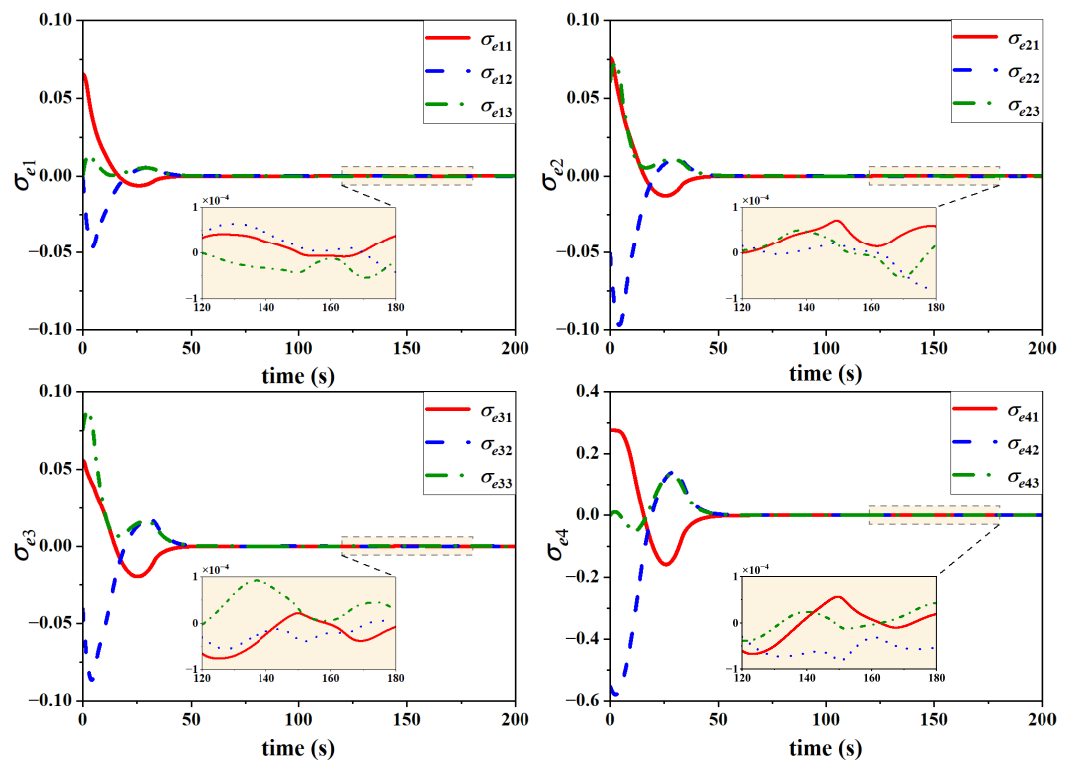


Figure 3. Attitude tracking error trajectories of four spacecraft.

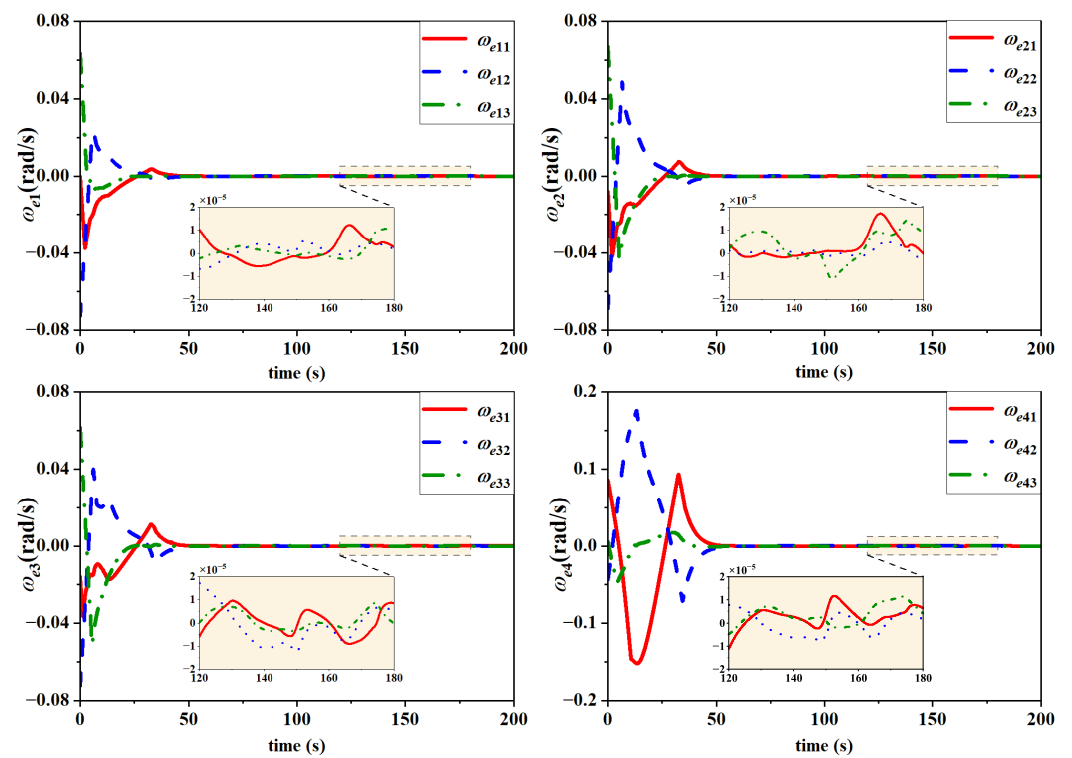


Figure 4. Attitude angle velocity tracking error trajectories of four spacecraft.

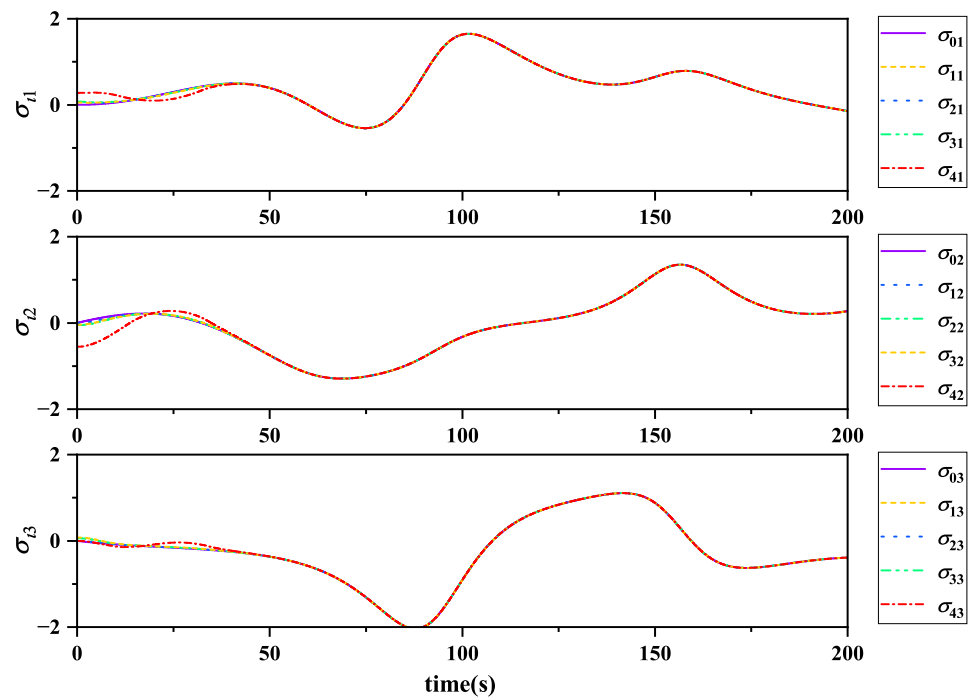


Figure 5. Attitude MRPs synchronization performance of four spacecraft.

The parameters  $k = 0.2$ ,  $k_1 = 10$  and  $k_2 = 1.5$  are designed to drive the sliding mode vector onto the sliding manifold and ensure that the state variable finally evolves into a neighborhood of the equilibrium point. The fractional-order sliding mode tuned by  $k_2$  is utilized to accelerate the convergence of  $s_i$ . The control torques are illustrated in Figure 6, in which the input saturation constraint  $u_{i,k} \leq 0.3(\text{Nm})$  is clearly seen. The output torque upper bound  $u_{i,k,\max}$  reveals the control capacity of the actuator and determines the convergence rate to a large extent.

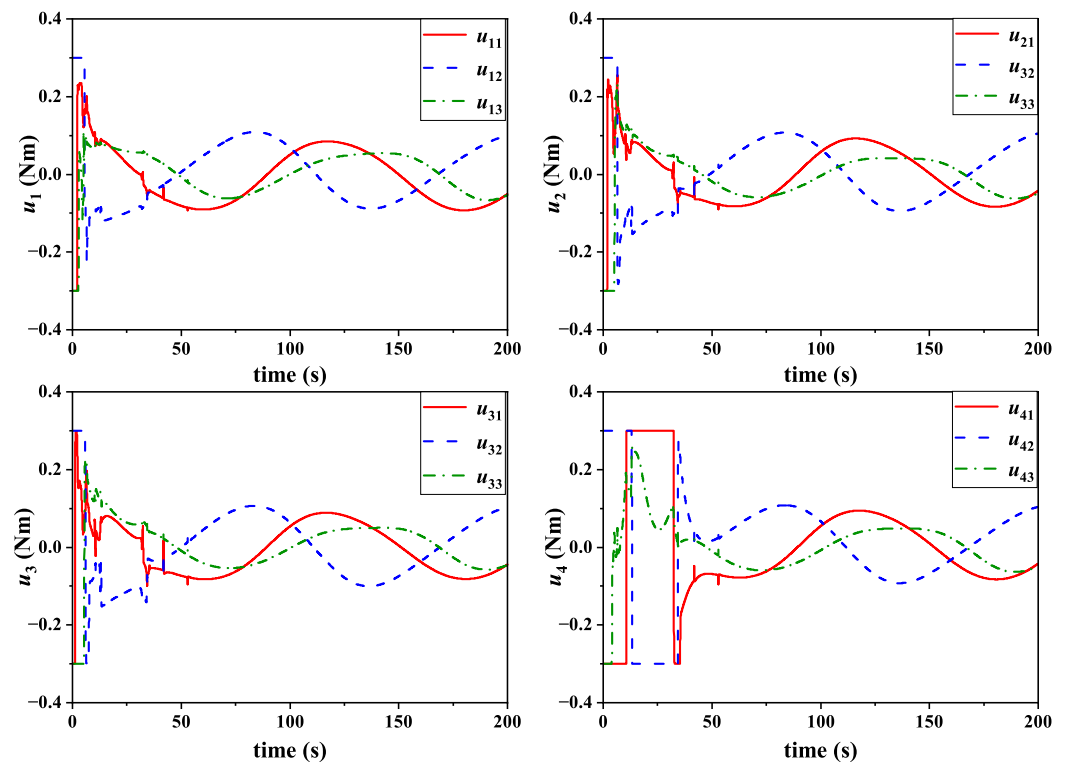


Figure 6. Control torques of four spacecraft.

The parameters  $\eta$ ,  $\beta$  and  $\gamma$  are related to the update rate of the adaptive parameters  $\widehat{M}_i$  and  $\chi_i$ ; their values are selected as  $\eta = 0.01$ ,  $\beta = 100$ ,  $\gamma = 0.001$ . The adaptive parameters  $\widehat{M}_i$  and  $\chi_i$  are initialized as zero. Figure 7 demonstrates the evolution trajectories of  $\chi_i$ , which shows that each element of  $\chi_i$  converges to constant individually and confirms the boundedness of  $\chi_i$ .

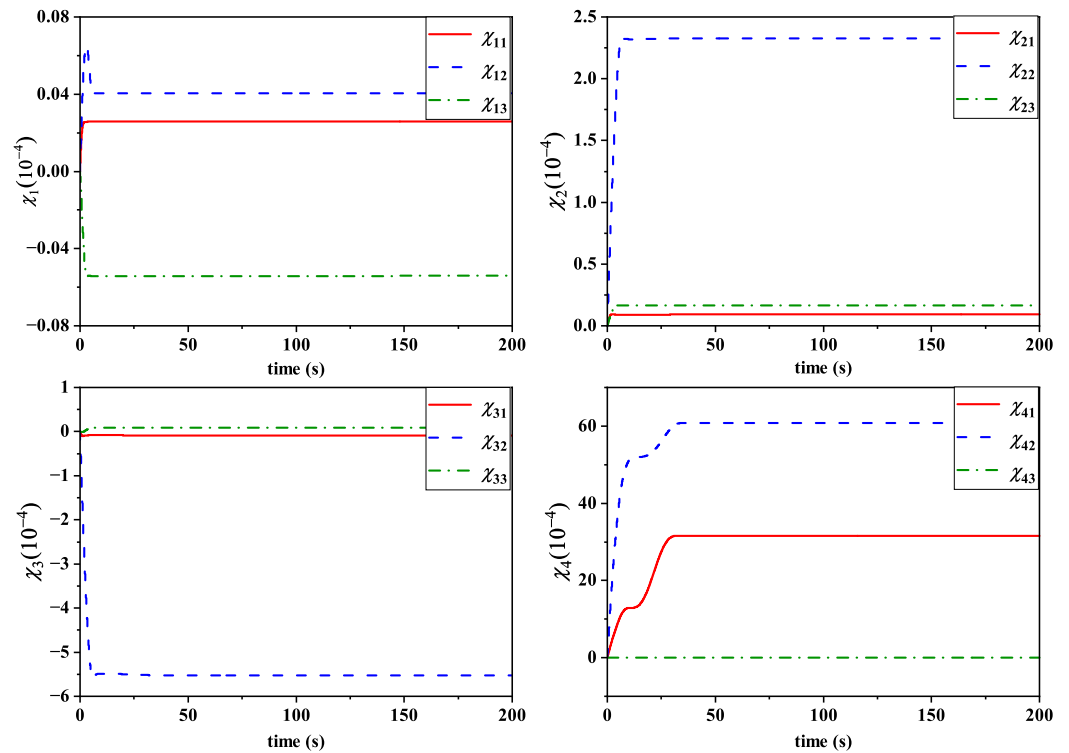
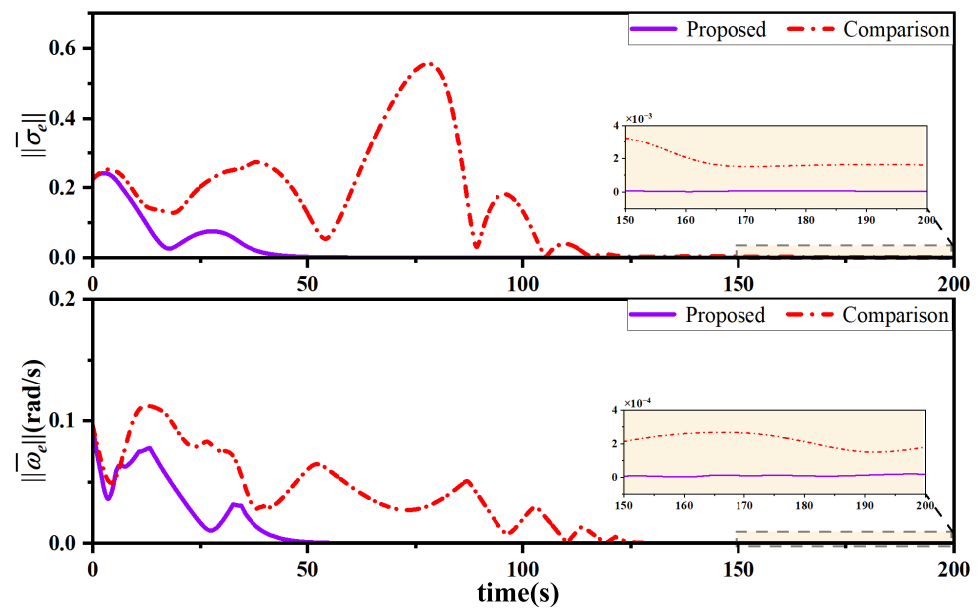


Figure 7. The evolution trajectories of adaptive parameter  $\chi_i$ .

With the parameters  $k_\epsilon = 0.5$ ,  $k_\mu = 1$ ,  $\zeta = 1$  and  $\mu_{i,max} = 0.005$ , the variable structure adaptive ChNN-based approximator can estimate the bounded nonlinear terms and uncertainties online. The parameters  $k_\epsilon$ ,  $k_\mu$ ,  $\zeta$  belonging to the hyperbolic tangent function not only have an impact on the control accuracy, but can also effectively alleviate the chattering caused by the signum function. As mentioned earlier, to make up for the poor approximation ability at the learning phase of the ChNN, the adaptive ChNN-based approximator takes effect only when  $\|\widehat{M}_i T_i\| \leq \mu_{i,max}$ ; its functional effect is reflected by the switching function  $m_i(t)$ . In addition, a filter  $G(s) = 1/(Ts + 1)$ ,  $T = 0.1$  acting on  $m_i(t)$  can be introduced to relieve the chattering caused by  $m_i(t)$ .

In order to confirm the control performance of the proposed ChNN-based controller, a comparative simulation between the presented controller and the controller in [3] is performed. The simulations are carried out under the same condition and parameters are chosen the same values as mentioned above. The control parameters in [3] are chosen as  $\beta = 1$ ,  $\beta_{i1} = 0.01$ ,  $\beta_{i2} = 80$ ,  $\beta_{i4} = 0.1$ ,  $k_i = 200$ , and the output torque is also bound by  $u_{i,k,max} = 0.3$  Nm. Figure 8 illustrates the evolution trajectories of  $\|\bar{\sigma}_e\|$  and  $\|\bar{\omega}_e\|$ , where  $\bar{\sigma}_e$  and  $\bar{\omega}_e$  are the averaged attitude tracking error and the averaged angular velocity tracking error, respectively. Simulation results show that the proposed controller can ensure the state variables converging to the equilibrium with a faster convergence speed and higher accuracy than the comparison controller. The major cause of control performance differences is the way of dealing with actuator saturation.



**Figure 8.** The Euclidean norm evolution trajectories of averaged attitude tracking error  $\bar{\sigma}_e$  and averaged angular velocity tracking error  $\bar{\omega}_e$ .

Although simulation results show fine performance of the proposed controller, there still exists some limitations: (1) The research is conducted with an undirected communication graph and the study on multi-spacecraft consensus control is also not comprehensive. In future studies, the consensus problem under directed graph should be substantially investigated. (2) In this paper, the proposed method introduces a ChNN to approximate nonlinearities of the closed-loop system; however, limited by its single-layer neuron structure, the approximation ability of ChNN is not powerful enough. The combination of control theory and intelligent learning needs to be further explored.

## 6. Conclusions

In this paper, the attitude synchronization and tracking problem subject to input saturation of spacecraft formation has been investigated and a promising distributed control scheme is proposed. An adaptive ChNN-based approximator is used to estimate the uncertainties caused by the bounded external disturbances, inertia uncertainties and other unknown nonlinear function online. A switch function is utilized to bound the output of the ChNN and serves as a switching signal between the adaptive ChNN control and robust control law. An auxiliary system based on a Nussbaum-type function and smooth hyperbolic tangent function is designed to handle the impact of input saturation. Lyapunov's stability method is applied for stability analysis of the closed-loop system and finally, numerical simulations are performed and the results validate the effectiveness and robustness of the proposed control scheme, the attitude of each individual spacecraft convergences to the reference attitude in spite of external disturbance and inertia uncertainties with constrained actuator control magnitude.

**Author Contributions:** Z.F.: Conceptualization, methodology, software and writing—original draft; J.W.: Conceptualization, methodology and writing—review and editing; N.W.: Validation and writing—review and editing; H.L.: Review and funding. All authors have read and agreed to the published version of the manuscript.

**Funding:** This work is supported by the Science Center Program of National Natural Science Foundation of China (Grant No.62188101), the National Natural Science Foundation of China (Grant No. 61833009, 61690212), the Heilongjiang Touyan Team, and the Guangdong Major Project of Basic and Applied Basic Research (Grant No. 2019B030302001).

**Conflicts of Interest:** The authors declare no conflict of interest.

## Nomenclature

The following abbreviations are used in this manuscript:

### Symbols

|                    |   |
|--------------------|---|
| $A$                | adjacency matrix                                |
| $B$                | connection matrix                               |
| $d_i$              | external disturbance vector, $N \cdot m$        |
| $u_i$              | control torque vector, $N \cdot m$              |
| $J_i$              | inertia tensor, $kg \cdot m^2$                  |
| $J_{0i}$           | nominal inertia tensor, $kg \cdot m^2$          |
| $L$                | Laplacian matrix                                |
| $S$                | multi-spacecraft sliding-mode vector            |
| $V$                | Lyapunov function                               |
| $\Delta J_i$       | inertia uncertainty, $kg \cdot m^2$             |
| $\Lambda$          | in-degree matrix                                |
| $\lambda_{di}$     | upper bound on the norm of external disturbance |
| $\lambda_{ji}$     | upper bound on the norm of inertia uncertainty  |
| $\lambda_{min}(A)$ | minimum eigenvalue of matrix $A$                |
| $\sigma_i$         | modified Rodriguez parameter vector             |
| $\sigma_{ei}$      | attitude (MRPs) tracking error                  |
| $\tau_i$           | commanded control signal, $N \cdot m$           |
| $\omega_i$         | angular velocity, rad/s                         |
| $\omega_{ei}$      | angular velocity tracking error, rad/s          |
| $\  \cdot \ $      | Euclidean norm                                  |
| $(\cdot)^\times$   | $3 \times 3$ vector cross-product matrix        |
| $\otimes$          | Kronecker product                               |

### Acronyms

|      |   |
|------|---|
| NN   | neural network                                |
| ChNN | Chebyshev neural network                      |
| SFF  | spacecraft formation flying                   |
| ASTC | attitude synchronization and tracking control |
| SMC  | sliding-mode control                          |
| MRPs | modified Rodriguez parameters                 |
| UUB  | uniformly ultimately bounded                  |

## References

- Dony, M.N.A.A.; Dong, W. Distributed Robust Formation Flying and Attitude Synchronization of Spacecraft. *J. Aerosp. Eng.* **2021**, *34*, 04021015. [[CrossRef](#)]
- Fan, L.; Huang, H. Coordinative coupled attitude and orbit control for satellite formation with multiple uncertainties and actuator saturation. *Acta Astronaut.* **2021**, *181*, 325–335. [[CrossRef](#)]
- Zhu, Z.; Guo, Y. Adaptive coordinated attitude control for spacecraft formation with saturating actuators and unknown inertia. *J. Frankl. Inst.* **2019**, *356*, 1021–1037. [[CrossRef](#)]
- Hu, Q.; Zhang, J.; Friswell, M.I. Finite-Time Coordinated Attitude Control for Spacecraft Formation Flying Under Input Saturation. *J. Dyn. Syst. Meas. Control.* **2015**, *137*, 061012. [[CrossRef](#)]
- Saeed Nasrolahi, S.; Abdollahi, F.; Rezaee, H. Decentralized active sensor fault tolerance in attitude control of satellite formation flying. *Int. J. Robust Nonlinear Control.* **2020**, *30*, 8340–8361. [[CrossRef](#)]
- Wu, B.; Wang, D.; Poh, E.K. Decentralized robust adaptive control for attitude synchronization under directed communication topology. *J. Guid. Control. Dyn.* **2011**, *34*, 1276–1282. [[CrossRef](#)]
- Yi, H.; Liu, M.; Li, M. Event-triggered fault tolerant control for spacecraft formation attitude synchronization with limited data communication. *Eur. J. Control.* **2019**, *48*, 97–103. [[CrossRef](#)]
- Cui, B.; Xia, Y.; Liu, K.; Zhang, J.; Wang, Y.; Shen, G. Truly Distributed Finite-Time Attitude Formation-Containment Control for Networked Uncertain Rigid Spacecraft. *IEEE Trans. Cybern.* **2020**, *52*, 5882–5896. [[CrossRef](#)]
- Zhu, Z.; Guo, Y.; Gao, Z. Adaptive finite-time actuator fault-tolerant coordinated attitude control of multispacecraft with input saturation. *Int. J. Adapt. Control. Signal Process.* **2019**, *33*, 644–663. [[CrossRef](#)]
- Wang, W.; Li, C.; Sun, Y.; Ma, G. Distributed coordinated attitude tracking control for spacecraft formation with communication delays. *ISA Trans.* **2019**, *85*, 97–106. [[CrossRef](#)]
- Zou, A.; de Ruiter, A.H.; Kumar, K.D. Distributed finite-time velocity-free attitude coordination control for spacecraft formations. *Automatica* **2016**, *67*, 46–53. [[CrossRef](#)]

12. Chen, T.; Shan, J. Continuous constrained attitude regulation of multiple spacecraft on SO(3). *Aerosp. Sci. Technol.* **2020**, *99*, 105769. [[CrossRef](#)]
13. Zhang, Z.; Zhang, Z.; Zhang, H. Distributed attitude control for multispacecraft via Takagi–Sugeno fuzzy approach. *IEEE Trans. Aerosp. Electron. Syst.* **2017**, *54*, 642–654. [[CrossRef](#)]
14. Du, H.; Li, S. Attitude synchronization for flexible spacecraft with communication delays. *IEEE Trans. Autom. Control.* **2016**, *61*, 3625–3630. [[CrossRef](#)]
15. Nazari, M.; Butcher, E.A.; Yucelen, T.; Sanyal, A. K Decentralized consensus control of a rigid-body spacecraft formation with communication delay. *J. Guid. Control. Dyn.* **2016**, *39*, 838–851. [[CrossRef](#)]
16. Zou, Y.; Meng, Z. Velocity-free leader-follower cooperative attitude tracking of multiple rigid bodies on SO(3). *IEEE Trans. Cybern.* **2019**, *39*, 4078–4089. [[CrossRef](#)]
17. Lu, K.; Li, T.; Zhang, L. Active attitude fault-tolerant tracking control of flexible spacecraft via the Chebyshev neural network. *Trans. Inst. Meas. Control* **2019**, *41*, 925–933. [[CrossRef](#)]
18. Xia, R.; Chen, M.; Wu, Q. Neural network based optimal adaptive attitude control of near-space vehicle with system uncertainties and disturbances. *Proc. Inst. Mech. Eng. Part G J. Aerosp. Eng.* **2019**, *233*, 641–656. [[CrossRef](#)]
19. Shi, X.; Zhou, D.; Chen, X.; Zhou, Z. Actor-critic-based predefined-time control for spacecraft attitude formation system with guaranteeing prescribed performance on SO(3). *Aerosp. Sci. Technol.* **2021**, *117*, 106898. [[CrossRef](#)]
20. Cai, H.; Huang, J. Leader-following attitude consensus of multiple rigid body systems by attitude feedback control. *Automatica* **2016**, *69*, 87–92. [[CrossRef](#)]
21. Hou, Z.; Zou, A.; Cheng, L.; Tan, M. Adaptive control of an electrically driven nonholonomic mobile robot via backstepping and fuzzy approach. *IEEE Trans. Control. Syst. Technol.* **2009**, *17*, 803–815.
22. Li, A.; Liu, M.; Shi, Y. Adaptive sliding mode attitude tracking control for flexible spacecraft systems based on the Takagi-Sugeno fuzzy modelling method. *Acta Astronaut.* **2020**, *175*, 570–581. [[CrossRef](#)]
23. Zhao, L.; Yu, J.; Shi, P. Command filtered backstepping-based attitude containment control for spacecraft formation. *IEEE Trans. Syst. Man, Cybern. Syst.* **2019**, *51*, 1278–1287. [[CrossRef](#)]
24. Amrr, S.M.; Alturki, A.; Kumar, A.; Nabi, M. Prescribed Performance-Based Event-Driven Fault-Tolerant Robust Attitude Control of Spacecraft under Restricted Communication. *Electronics* **2021**, *10*, 1709. [[CrossRef](#)]
25. Liang, Y.; Ting, L.; Lin, L. Study of reliable control via an integral-type sliding mode control scheme. *IEEE Trans. Ind. Electron.* **2012**, *59*, 3062–3068. [[CrossRef](#)]
26. Defoort, M.; Floquet, T. A novel higher order sliding mode control scheme. *Syst. Control. Lett.* **2009**, *58*, 102–108. [[CrossRef](#)]
27. Wu, F.; Liu, M.; Feng, Z.; Cao, X. Fractional-order sliding mode attitude coordinated control for spacecraft formation flying with unreliable wireless communication. *IET Control. Theory Appl.* **2022**.. [[CrossRef](#)]
28. Tang, G.; Dong, R.; Gao, H. Optimal sliding mode control for nonlinear systems with time-delay. *Nonlinear Anal. Hybrid Syst.* **2008**, *2*, 891–899. [[CrossRef](#)]
29. Hornik, K.; Stinchcombe, M.; White, H. Multilayer feedforward networks are universal approximators. *Neural Netw.* **1989**, *2*, 359–366. [[CrossRef](#)]
30. Zou, A.; Kumar, K.D.; Hou, Z.G. Quaternion-based adaptive output feedback attitude control of spacecraft using Chebyshev neural networks. *IEEE Trans. Neural Netw.* **2010**, *21*, 1457–1471.
31. Zou, A.; Kumar, K.D.; Hou, Z.; Liu, X. Finite-time attitude tracking control for spacecraft using terminal sliding mode and Chebyshev neural network. *IEEE Trans. Syst. Man Cybern. Part B* **2011**, *41*, 950–963.
32. Yu, B.; Du, H.; Ding, L.; Wu, D.; Li, H. Neural network-based robust finite-time attitude stabilization for rigid spacecraft under angular velocity constraint. *Neural Comput. Appl.* **2022**, *34*, 5107–5117. [[CrossRef](#)]
33. Ali, I.; Radice, G.; Kim, J. Backstepping control design with actuator torque bound for spacecraft attitude maneuver. *J. Guid. Control. Dyn.* **2010**, *33*, 254–259. [[CrossRef](#)]
34. Gui, H.; Vukovich, G. Finite-time angular velocity observers for rigid-body attitude tracking with bounded inputs. *Int. J. Robust Nonlinear Control* **2017**, *27*, 15–38. [[CrossRef](#)]
35. Wang, L.; Guo, Y.; Ma, G.; Weilin, L. Review on Input Saturation in the Spacecraft Attitude Control. *J. Astronaut.* **2021**, *42*, 11–21.
36. Hu, Q.; Tan, X.; Akella, M.R. Finite-Time Fault-Tolerant Spacecraft Attitude Control with Torque Saturation. *J. Guid. Control. Dyn.* **2017**, *40*, 2524–2537. [[CrossRef](#)]
37. Gao, S.; Jing, Y.; Liu, X.; Zhang, S. Finite-time attitude-tracking control for rigid spacecraft with actuator failures and saturation constraints. *Int. J. Robust Nonlinear Control* **2020**, *30*, 1903–1937. [[CrossRef](#)]
38. Ding, Z. Adaptive consensus output regulation of a class of nonlinear systems with unknown high-frequency gain. *Automatica* **2015**, *51*, 348–355. [[CrossRef](#)]
39. Khettab, K.; Ladaci, S.; Bensafia, Y. Fuzzy adaptive control of fractional order chaotic systems with unknown control gain sign using a fractional order Nussbaum gain. *IEEE/CAA J. Autom. Sin.* **2016**, *6*, 816–823. [[CrossRef](#)]
40. Wen, C.; Zhou, J.; Liu, Z.; Su, H. Robust adaptive control of uncertain nonlinear systems in the presence of input saturation and external disturbance. *IEEE Trans. Autom. Control.* **2011**, *56*, 1672–1678. [[CrossRef](#)]
41. Ji, N.; Liu, J. Vibration control for a flexible satellite with input constraint based on Nussbaum function via backstepping method. *Aerosp. Sci. Technol.* **2018**, *77*, 563–572. [[CrossRef](#)]

42. Hu, Q.; Shao, X.; Guo, L. Adaptive fault-tolerant attitude tracking control of spacecraft with prescribed performance. *IEEE/ASME Trans. Mechatronics* **2017**, *23*, 331–341. [[CrossRef](#)]
43. Schaub, H.; Junkins, J.L. Stereographic orientation parameters for attitude dynamics: A generalization of the Rodrigues parameters. *J. Astronaut. Sci.* **1996**, *44*, 1–19.
44. Schaub, H.; Junkins, J.L. *Analytical Mechanics of Space Systems*; AIAA: Reston, VA, USA, 2003.
45. Wallsgrove, R.J.; Akella, M.R. Globally stabilizing saturated attitude control in the presence of bounded unknown disturbances. *J. Guid. Control. Dyn.* **2005**, *28*, 957–963. [[CrossRef](#)]
46. West, D.B. *Introduction to Graph Theory*; Prentice-Hall: Upper Saddle River, NJ, USA, 2001.
47. Nussbaum, R.D. Some remarks on a conjecture in parameter adaptive control. *Syst. Control. Lett.* **1983**, *3*, 243–246. [[CrossRef](#)]
48. Ao, W.; Huang, J. Adaptive leaderless consensus control of a class of strict-feedback nonlinear multi-agent systems with unknown control directions: A non-Nussbaum function based approach. *J. Frankl. Inst.* **2020**, *357*, 12180–12196. [[CrossRef](#)]
49. Ioannou, P.A.; Sun, J. *Robust Adaptive Control*; Prentice-Hall: Upper Saddle River, NJ, USA, 1996.
50. Horn, R.A.; Johnson, C.R. *Topics in Matrix Analysis*; Cambridge University Press: Cambridge, UK, 1991.
51. Horn, R.A.; Johnson, C.R. *Matrix Analysis*; Cambridge University Press: Cambridge, UK, 1985.
52. Zhihong, M.; Paplinski, A.P.; Wu, H.R. A robust MIMO terminal sliding mode control scheme for rigid robotic manipulators. *IEEE Trans. Autom. Control* **1994**, *39*, 2464–2469. [[CrossRef](#)]